

Space-time evolution of particle emission in p–Pb collisions at $\sqrt{s_{\text{NN}}} = 5.02$ TeV with 3D kaon femtoscopy



The ALICE collaboration

Full author list at the end of the paper

E-mail: ALICE-publications@cern.ch

ABSTRACT: The measurement of three-dimensional femtosopic correlations between identical charged kaons ($K^{\pm}K^{\pm}$) produced in p–Pb collisions at center-of-mass energy per nucleon pair $\sqrt{s_{\text{NN}}} = 5.02$ TeV with ALICE at the LHC is presented for the first time. This measurement, supplementary to those in pp and Pb–Pb collisions, allows understanding the particle-production mechanisms at different charged-particle multiplicities and provides information on the dynamics of the source of particles created in p–Pb collisions, for which a general consensus does not yet exist. It is shown that the measured source sizes increase with charged-particle multiplicity and decrease with increasing pair transverse momentum. These trends for $K^{\pm}K^{\pm}$ are similar to the ones observed earlier in identical charged-pion and $K_s^0K_s^0$ correlations in Pb–Pb collisions at various energies and in $\pi^{\pm}\pi^{\pm}$ correlations in p–Pb collisions at $\sqrt{s_{\text{NN}}} = 5.02$ TeV. At comparable multiplicity, the source sizes measured in p–Pb collisions agree within uncertainties with those observed in pp collisions, and there is an indication that they are smaller than those observed in Pb–Pb collisions. The obtained results are also compared with predictions from the hadronic interaction model EPOS 3, which tends to underestimate the source size for the most central collisions and agrees with the data for semicentral and peripheral events. Furthermore, the time of maximal emission for kaons is extracted. It turns out to be comparable with the value obtained in highly peripheral Pb–Pb collisions at the same energy, indicating that the kaon emission evolution is similar to that in p–Pb collisions.

KEYWORDS: Heavy Ion Experiments, Particle Correlations and Fluctuations, Relativistic Heavy Ion Physics

ARXIV EPRINT: [2601.15081](https://arxiv.org/abs/2601.15081)

Contents

1	Introduction	1
2	Data analysis	3
2.1	Event classification	4
2.2	Particle and pair selection	4
2.3	Purity	6
3	Measurement and parametrization of the correlation function	6
3.1	Fitting 1D correlation function	8
3.2	Fitting 3D correlation function	8
4	Systematic uncertainties	10
5	Results and discussion	12
5.1	1D analysis results	12
5.2	3D analysis results	15
6	Summary	19
	The ALICE collaboration	28

1 Introduction

During its operation, the Large Hadron Collider (LHC) [1] delivered pp, p–Pb, and Pb–Pb collisions at various energies, which have been used to study the properties of matter created in such environments. Signatures of quark-gluon plasma (QGP) formation were observed in Pb–Pb collisions, such as a strong suppression of high-momentum particle production (jet quenching) [2–4], a suppression of the $K^*(892)^0/K$ yield ratio [5, 6], strangeness enhancement [7, 8], Debye screening effect [9–12], or collective flow effects [13, 14], which are well described by hydrodynamic models [15–17]. As shown by the comparison of the Pb–Pb results to reference pp measurements, these effects could not be described by a simple incoherent superposition of nucleon–nucleon interactions and could be interpreted as final-state phenomena, characteristic to QGP creation in heavy-ion collisions [18–22]. Since an extended QGP phase is not expected to form in proton–nucleus collision systems, the comparison of the p–Pb results to the Pb–Pb ones might help select observables that could be used to understand the mechanism and conditions of QGP formation in high-energy collisions.

The femtoscopy technique [23–26], which studies particle correlations in momentum space, is an effective tool for extracting the size of the particle-emitting region at freeze-out [27] (conventionally called the “radius” parameter) and the decoupling time of matter created in relativistic collisions. Strictly speaking, by using femtoscopy one can measure not the whole volume of the particle emitting source but the size of the region of an expanding source from which the particles with similar momenta are emitted [28, 29], the so-called

“homogeneity volume”. This volume is smaller than the total volume of the system and decreases with increasing pair transverse momentum $k_T = |\mathbf{p}_{T,1} + \mathbf{p}_{T,2}|/2$ or transverse mass $m_T = \sqrt{m^2 + k_T^2}$ (for particles with identical masses m and transverse momenta $\mathbf{p}_{T,1}$ and $\mathbf{p}_{T,2}$). Thus, the femtoscopic correlations can be used to measure the spatial and temporal information of the particle emitting source allowing for extraction of the dynamic information on the emission process.

In the one-dimensional (1D) femtoscopic analysis, the source, in the pair rest frame, is characterized by one size parameter R_{inv} [26]. Several 1D analyses were performed at the LHC for correlations of various particle species in pp [30–34], p–Pb [35, 36], and Pb–Pb collisions [37–39]. Since the 1D analysis can be performed even with a small amount of collected experimental data, it can be done in almost any experiment and for various types of particles. However, the information obtained in this kind of analysis is limited by extracting a generalized size, and no information on the shape of the source can be obtained. In the more general case, the shape of the source can be retrieved in the three-dimensional (3D) analysis where its size is determined independently for three directions: “long” (R_{long}) along the beam direction (z axis of the reference frame), “out” (R_{out}) along the pair transverse momentum, and “side” (R_{side}), perpendicular to the other two. For high-energy collisions, analyses are usually performed in the longitudinally comoving system (LCMS), a rest frame moving along the beam direction such that the pair total momentum projection P_z vanishes, i.e. $P_z = P_{1,z} + P_{2,z} = 0$ [26]. The 3D analysis requires more experimental data and, therefore, is often performed for the most abundantly produced particles, i.e. charged pions [40–42]. For kaons, the second most copiously produced particles, all 3D femtoscopic analyses that have been done by now are for heavy-ion collisions [43–45]. For proton–nucleus collision systems, for example p–Pb collisions, only a few 1D femtoscopic analyses have been performed so far [35, 46]. The study of femtoscopic correlations in such systems is particularly interesting because it provides a bridge between small (pp) and large (A–A) collision systems, and may lead to additional constraints on model scenarios that successfully describe pp and A–A collisions. While the A–A results can be interpreted within the hydrodynamic framework [26, 47, 48], and the pp data are explained by a hydrodynamic expansion [49] taking into account additional effects related to the uncertainty principle [50], there is no common interpretation of the results obtained in collisions where one of the colliding projectiles is a particle. Some studies [36, 51, 52] suggest that a hydrodynamic evolution similar to that for A–A collisions may be present in such systems. However, as shown in refs. [35, 38, 41], the radii for the p–Pb system, at a given track multiplicity, were found to be closer in magnitude to those in pp, while there was a visible gap separating the radii in p–Pb and Pb–Pb collisions. This may demonstrate the influence of different initial conditions on the final-state, or indicate significant collective expansion already in peripheral Pb–Pb collisions.

In this work, 1D and 3D femtoscopic correlations of two identical charged kaons $K^\pm K^\pm$ are studied in p–Pb collisions at $\sqrt{s_{\text{NN}}} = 5.02$ TeV. Identical-kaon femtoscopy gives information about the collision region that is complementary to that obtained with identical-pion femtoscopy. It probes the hotter region of the particle emitting source, where strange quarks are produced, and extends the momentum range over which the femtoscopy analysis can be applied. The kaon analysis also offers a cleaner signal compared to pions, as it is less

affected by resonance decays. The kaon femtoscopic radii as a function of the pair transverse momentum, which are reported in this article, provide additional constraints on the validity of approaches used to describe matter created in ultrarelativistic collisions. Comparison of femtoscopic characteristics in different collision systems, such as pp, p–Pb, and Pb–Pb, and with EPOS 3.111 model [53] calculations allows investigating the dynamics of high-energy collision evolution and also helps tune and constrain the model parameters. Fitting the m_T dependence of R_{long}^2 in the LCMS [54, 55] with the function suggested in refs. [56, 57], the duration of the collision evolution characterized by the time of maximal emission can be estimated. It was shown in the analysis of identical charged kaon correlations in Pb–Pb collisions at $\sqrt{s_{\text{NN}}} = 5.02$ TeV [58] and its comparison with the integrated hydrokinetic model (iHKM) calculations [59] that the system created in peripheral collisions evolves faster than in central ones. In the presented analysis, the time of maximal emission for kaons τ_K was extracted from the experimental data for an asymmetric collision system, namely p–Pb, to understand the particle emission dynamics by comparing these results with those obtained in Pb–Pb collisions.

The article is organized as follows: Section 2 describes the ALICE apparatus, the analyzed data sample, and the event- and track-selection criteria. The details of the femtoscopic correlation function analysis presented in this work are given in section 3. The associated systematic uncertainties are discussed in section 4. The obtained results are shown and compared with model predictions in section 5 and summarized in section 6.

2 Data analysis

The data sample studied in this work was collected in 2016 by ALICE from p–Pb collisions at a center-of-mass energy per nucleon–nucleon pair of $\sqrt{s_{\text{NN}}} = 5.02$ TeV during the LHC Run 2 period. The nucleon–nucleon center-of-mass system is shifted with respect to the ALICE laboratory system by 0.465 units of rapidity in the direction of the proton beam [60]. Throughout this paper η represents the pseudorapidity measured in the laboratory frame.

In the LHC Run 2 period, the ALICE apparatus consisted of a central barrel, covering the pseudorapidity region $|\eta| < 0.9$, a muon spectrometer with $-4.0 < \eta < -2.5$ coverage, and forward- and backward-pseudorapidity detectors employed for triggering, background rejection, and event characterization. An overview of the detector and its performance are presented in refs. [22, 61, 62].

Approximately 250×10^6 minimum-bias events were analyzed. They were obtained using the minimum-bias trigger provided by the V0 detector [63], which is composed of two scintillator arrays placed on either side of the interaction point along the beam axis with pseudorapidity coverage $2.8 < \eta < 5.1$ (V0A, located on the Pb remnant side) and $-3.7 < \eta < -1.7$ (V0C). The minimum-bias trigger requires a signal in both V0 detectors within a time window that is consistent with the collision occurring at the center of the ALICE detector. The V0 detector was also utilized for determining the multiplicity of the analyzed events [64] using the measured energy deposition. The multiplicity classes were defined in terms of percentile intervals of the measured V0A amplitude [65]. The central barrel detectors used in the analysis are the Inner Tracking System (ITS) [66, 67], the Time Projection Chamber (TPC) [68, 69], and the Time-Of-Flight detector (TOF) [70–72]. They

are embedded in a large solenoidal magnet that provides a magnetic field of 0.5 T parallel to the beams axis. The ITS consists of six layers of silicon detectors and was used to reconstruct the primary vertex and to track charged particles. The TPC is the main tracking detector of the central barrel. It is a gaseous detector placed co-axially with the beam axis and radially next to the ITS. It is divided by a central electrode into two halves. The end caps on either side are composed of 18 sectors (covering the full azimuthal angle) with 159 pad rows placed radially in each sector. A track signal in the TPC consists of space points (clusters), each of which is reconstructed in one of the pad rows. It also enables charged-particle identification via the measurement of the particle specific energy loss (dE/dx) in the detector gas. The TPC covers an acceptance of $|\eta| < 0.9$ for tracks that reach the outer radius of the detector and $|\eta| < 1.5$ for shorter tracks. The TOF is a gaseous detector, which uses multigap resistive plate chambers [73] as its basic detecting element. The primary-vertex position was determined with tracks reconstructed in the ITS and TPC, as described in ref. [74]. In order to obtain a uniform acceptance of the detectors, only events with a reconstructed primary vertex within ± 10 cm from the center of the detector along the beam direction z were included in the analysis. The parameters of each track are determined by performing a Kalman fit to a set of clusters with an additional constraint for the track to pass through the primary vertex. The fit was required to deliver χ^2/NDF less than 2. The transverse momentum of each track was determined from its curvature in the magnetic field. The particle identification capabilities of the TPC are supplemented with the TOF detector, which provides a measurement of the time of flight of charged particles.

2.1 Event classification

The 1D analysis was conducted in two different variants. The first was performed in six multiplicity classes [64, 65]: 0–5%, 5–10%, 10–20%, 20–40%, 40–60%, and 60–80% and two pair transverse momentum k_T ranges: (0.2–0.5) and (0.5–1.0) GeV/ c for a finer comparison with the results from pp [32] and Pb–Pb [37, 58] collision systems and also for crosscheck with the results of the previous p–Pb analysis [35]. The second was done in three multiplicity classes: 0–20%, 20–40%, and 40–90% and in eight k_T ranges: (0.2–0.3), (0.3–0.4), (0.4–0.5), (0.5–0.6), (0.6–0.7), (0.7–0.8), (0.8–1.0), and (1.0–1.3) GeV/ c to better study the trend with k_T and to have a more detailed comparison with the EPOS 3 calculations. The 3D analysis was performed in three multiplicity classes: 0–20%, 20–40%, and 40–90% and two k_T ranges: (0.2–0.5) and (0.5–1.0) GeV/ c .

Tables 1 and 2 show the mean charged-particle multiplicity densities $\langle dN_{\text{ch}}/d\eta \rangle$ averaged over $|\eta| < 0.5$ using the method presented in ref. [64] for the analyses in six and three multiplicity classes, respectively. The $\langle dN_{\text{ch}}/d\eta \rangle$ values were not corrected for trigger and vertex-reconstruction inefficiency, which is about 4% for non-single diffractive events [75].

2.2 Particle and pair selection

The identification of kaons was conducted employing both the TPC and the TOF detectors by applying a strict selection on the deviation n_σ between the measured quantities (dE/dx and time-of-flight) and the expected values for a kaon, normalized by the detector resolution σ . The n_σ thresholds were chosen so as to remove possible contamination from electrons,

Event class	$\langle dN_{\text{ch}}/d\eta \rangle, \eta < 0.5$
0–5%	45.0 ± 1.0
5–10%	36.2 ± 0.8
10–20%	30.5 ± 0.7
20–40%	23.2 ± 0.5
40–60%	16.1 ± 0.4
60–80%	9.8 ± 0.2

Table 1. Event multiplicity classes and their corresponding $\langle dN_{\text{ch}}/d\eta \rangle$ [64] for the analysis in six multiplicity intervals as obtained using the method presented in ref. [75]. The given uncertainties are systematic only, the statistical uncertainties are negligible.

Event class	$\langle dN_{\text{ch}}/d\eta \rangle, \eta < 0.5$
0–20%	35.6 ± 0.8
20–40%	23.2 ± 0.5
40–90%	12.9 ± 0.3

Table 2. Event multiplicity classes and their corresponding $\langle dN_{\text{ch}}/d\eta \rangle$ [64] for the analysis in three multiplicity intervals as obtained using the method presented in ref. [75]. The given uncertainties are systematic only, the statistical uncertainties are negligible.

pions, and protons to the kaon sample. The kaon candidates were selected within a transverse momentum range of $0.14 < p_T < 1.50 \text{ GeV}/c$ and a pseudorapidity range of $|\eta| < 0.8$, to avoid regions of the detector with limited acceptance. To significantly improve the amount of primary kaons with respect to secondary particles coming from weak decays and particle-detector interactions, a selection criterion on the distance of closest approach (DCA) to the primary vertex was applied, both in the transverse plane ($\text{DCA}_{xy} < 0.135 \text{ cm}$) and along the direction of the beam ($\text{DCA}_z < 0.13 \text{ cm}$). Tracks reconstructed in the TPC were selected based on the criteria listed in table 3, which are similar to those used in the analysis described in ref. [35]. To ensure a good momentum resolution, each track was required to be composed of at least 80 out of the maximum possible 159 TPC clusters. Charged-particle tracks with momentum $p < 0.5 \text{ GeV}/c$ were identified as kaons if they satisfied the requirement $|n_{\sigma, \text{TPC}}| < 2$. Tracks with $p > 0.5 \text{ GeV}/c$ were required to match to a signal in the TOF, and satisfy $|n_{\sigma, \text{TPC}}| < 3$ as well as the following momentum-dependent $n_{\sigma, \text{TOF}}$ selection: $|n_{\sigma, \text{TOF}}| < 2$ for $0.5 < p < 0.8 \text{ GeV}/c$, $|n_{\sigma, \text{TOF}}| < 1.5$ for $0.8 < p < 1.0 \text{ GeV}/c$, and $|n_{\sigma, \text{TOF}}| < 1$ for $1.0 < p < 1.5 \text{ GeV}/c$.

As discussed in detail in ref. [40], the femtoscopic correlation functions of two identical particles are sensitive to two-track reconstruction effects when the particles are close in momentum and have close trajectories. Two kinds of two-track effects were investigated in this work. Track “splitting” occurs when one track is mistakenly reconstructed as two. Track “merging” corresponds to the reconstruction of two different tracks as one when they cannot be distinguished if their trajectories stay close to each other through a significant part of the TPC volume. To suppress such cases, each cluster in the TPC was flagged as “shared” if it was used in the reconstruction of more than one track, and pairs that shared $> 5\%$ of

Selection criterium	Value
p_T	$0.14 < p_T < 1.5 \text{ GeV}/c$
$ \eta $	< 0.8
DCA_{xy}	$< 0.135 \text{ cm}$
DCA_z	$< 0.13 \text{ cm}$
$ n_{\sigma,\text{TPC}} $	< 2 (for $0.14 < p < 0.50 \text{ GeV}/c$) < 3 (for $p > 0.5 \text{ GeV}/c$)
$ n_{\sigma,\text{TOF}} $	< 2 (for $0.5 < p < 0.8 \text{ GeV}/c$) < 1.5 (for $0.8 < p < 1.0 \text{ GeV}/c$) < 1.0 (for $1.0 < p < 1.5 \text{ GeV}/c$)
Number of track points in TPC	≥ 80

Table 3. Charged kaon selection criteria.

clusters in the TPC were removed from the sample. In addition, the selected pairs of kaons were required to be separated on average in the TPC detector by at least 3 cm.

2.3 Purity

The kaon purity for $p < 0.5 \text{ GeV}/c$ was estimated as in ref. [35] by parametrizing the TPC dE/dx distribution of the experimental data in momentum slices and computing the fraction of particle species that could mistakenly contribute to the kaon signal. The purity of the kaon sample was defined as the fraction of accepted kaon tracks that correspond to true kaons. The dominant contamination for charged kaons comes from e^\pm in the momentum range $0.4 < p < 0.5 \text{ GeV}/c$. The parameters of the function fitting the TPC distribution in momentum slices depend on the fit interval and are the source of the systematic uncertainty associated with the estimated single kaon purity. The purity for $p > 0.5 \text{ GeV}/c$, where the TOF information was employed, was studied with DPMJET [76] simulations using GEANT 3 [77] to model particle transport through the detector. Based on the results of this study, the $n_{\sigma,\text{TOF}}$ thresholds were chosen to provide a single kaon purity greater than 99%. The momentum and multiplicity dependence of the single kaon purity in the region of maximal contamination is shown in figure 1 (left panel). The pair purity was calculated as the product of two single-particle purities for pairs with relative momentum $q_{\text{inv}} < 0.25 \text{ GeV}/c$ (q_{inv} is defined below in section 3), where the momenta were taken from the experimentally determined distribution. The obtained K^\pm pair purity as a function of k_T is shown in figure 1 (right panel). The pair purity is higher than the single-kaon one due to the effect of averaging over low- and high-momentum ranges in the full single-kaon momentum interval p (see ref. [35] for details).

3 Measurement and parametrization of the correlation function

The correlation function (CF) of two particles with momenta \mathbf{p}_1 and \mathbf{p}_2 is measured as a function of the momentum difference of the pair $\mathbf{q} = \mathbf{p}_1 - \mathbf{p}_2$ and can be expressed as the ratio

$$C(\mathbf{q}) = \frac{A(\mathbf{q})}{B(\mathbf{q})} \tag{3.1}$$

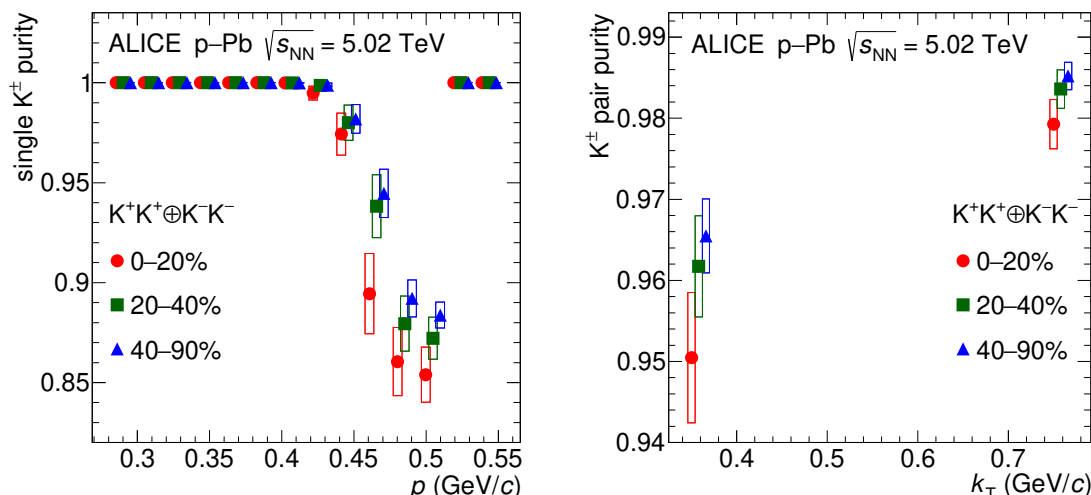


Figure 1. Single (left) and pair (right) K^\pm purities for different event multiplicity classes. The systematic uncertainties associated with the purity estimation are shown as boxes. Statistical uncertainties are negligible. The momentum p and k_T values for lower multiplicity classes (blue and green symbols) are slightly shifted for clarity.

of the two-particle distribution in a given event $A(\mathbf{q})$ to the reference distribution $B(\mathbf{q})$ [24]. The distribution $A(\mathbf{q})$ was constructed from the events having at least two identical charged kaons. The reference distribution was formed by mixing the events containing at least one charged kaon, where each event was mixed with five other events, which had similar z position (within 2 cm) of the primary vertex and similar multiplicity (within 1/4 of the width of the given multiplicity class) [26]. The correlation function C is normalized to unity such that $C \rightarrow 1$ in the absence of a correlation signal.

The 1D CF was calculated in the pair rest frame (where $\mathbf{p}_1 + \mathbf{p}_2 = 0$) as a function of the invariant relative momentum of the pair $q_{inv} = \sqrt{|\mathbf{q}|^2 - q_0^2}$, where $q_0 = E_1 - E_2$ and $\mathbf{q} = \mathbf{p}_1 - \mathbf{p}_2$ are determined by the energies E_1, E_2 and momenta $\mathbf{p}_1, \mathbf{p}_2$ of the particles, respectively. In the 3D femtoscopic analysis, the momentum difference \mathbf{q} was evaluated in the LCMS.

The correlation functions were corrected for purity according to [35, 37, 45] as

$$C_{corrected} = (C_{raw} - 1 + P)/P, \tag{3.2}$$

where the pair purity P depends on k_T and multiplicity, as shown as an example for the case of the 3D analysis in figure 1 (right panel).

The effect of finite track momentum resolution in the 1D analysis was accounted for through the use of a response matrix generated with DPMJET simulations and was applied on-the-fly during the fitting process (see section 3.1 below) as described in ref. [78]. In the 3D case, the correlation function was corrected for a momentum resolution factor evaluated with DPMJET simulations as the ratio of the CF as a function of the reconstructed relative momentum of the pair to the CF as a function of the true pair relative momentum. The details of the procedure can be found in ref. [45].

To extract information on the particle emitting source from the measured correlation function, the CFs are parametrized by various formulas depending on the origin of the

correlations between the considered particles. For the $K^\pm K^\pm$ case, they are quantum statistics and the Coulomb interaction. The effects in the CF due to strong final-state interactions between identical charged kaons are negligible given the shallow interaction [79].

3.1 Fitting 1D correlation function

Considering a Gaussian distribution for a spherical particle source in the pair rest frame (PRF), the fit of the 1D CF was performed using the Bowler-Sinyukov formula [29, 80]

$$C(q_{\text{inv}}) = N \left[1 - \lambda + \lambda K(r, q_{\text{inv}}) \left(1 + \exp \left(-R_{\text{inv}}^2 q_{\text{inv}}^2 \right) \right) \right] D(q_{\text{inv}}), \quad (3.3)$$

where $D(q_{\text{inv}})$ is a function used to parametrize all non-femtoscopic effects such as resonance decays or mini-jets [32, 40], and N is a normalization coefficient. The factor $K(r, q_{\text{inv}})$ describes the Coulomb interaction with a radius r evaluated according to refs. [80, 81] as

$$K(r, q_{\text{inv}}) = \frac{C_{\text{QS+Coulomb}}}{C_{\text{QS}}}, \quad (3.4)$$

where the theoretical correlation function C_{QS} takes into account quantum statistics (QS) only and $C_{\text{QS+Coulomb}}$ includes quantum statistical and Coulomb final-state interaction effects evaluated using the Lednický model [25]. The radius r determines the range of the Coulomb interaction used to calculate the $C_{\text{QS+Coulomb}}$ value. It was set to $r = 1.5$ fm, which is on average close to the radius values extracted in the presented analysis. Its uncertainty has systematic effects on the final results (as discussed in section 4 below).

The parameters R_{inv} and λ describe the size of the source and the correlation strength, respectively. They were extracted from the fit of eq. (3.3) to the data in the range of the correlation signal $0 < q_{\text{inv}} < 0.5$ GeV/ c handling the baseline $D(q_{\text{inv}})$ as described in ref. [35]. The non-femtoscopic effects were estimated with the EPOS 3 model [53] without QS nor Coulomb interaction effects included. The CF was normalized to unity outside the femtoscopic effect region, i.e. in the $0.25 < q_{\text{inv}} < 0.50$ GeV/ c range. The example 1D correlation functions can be found in ref. [35]. These CFs show all the features inherent in femtoscopic correlations of identical charged kaons in p-Pb collisions at $\sqrt{s_{\text{NN}}} = 5.02$ TeV, which are similar independently of the used multiplicity classes and k_{T} ranges.

3.2 Fitting 3D correlation function

To extract the information about the 3D size and shape of the particle emitting source, the 3D CF was fitted with the Bowler-Sinyukov formula (for a Gaussian-like source) [80, 82]

$$C(\mathbf{q}) = N \left[1 - \lambda + \lambda K(q_{\text{inv}}, R_{\text{inv}}) \left(1 + \exp \left(-R_{\text{out}}^2 q_{\text{out}}^2 - R_{\text{side}}^2 q_{\text{side}}^2 - R_{\text{long}}^2 q_{\text{long}}^2 \right) \right) \right] D(\mathbf{q}), \quad (3.5)$$

where q_{out} , q_{side} , and q_{long} are projections of the pair relative momentum \mathbf{q} in the LCMS, and R_{out} , R_{side} , and R_{long} are the corresponding femtoscopic source radii, with R_{out} related to the geometrical size of the emitting source and particle emission duration, R_{side} to the geometrical size, and R_{long} to the time of maximal emission. The parameters N , λ , $K(q_{\text{inv}}, R_{\text{inv}})$, and $D(q_{\text{out}}, q_{\text{side}}, q_{\text{long}})$ have the same meaning as in the 1D analysis in eq. (3.3). The normalization range was $0.3 < q_i < 0.4$ GeV/ c where $i = \text{out, side, long}$. The function $K(q_{\text{inv}}, R_{\text{inv}})$ is the

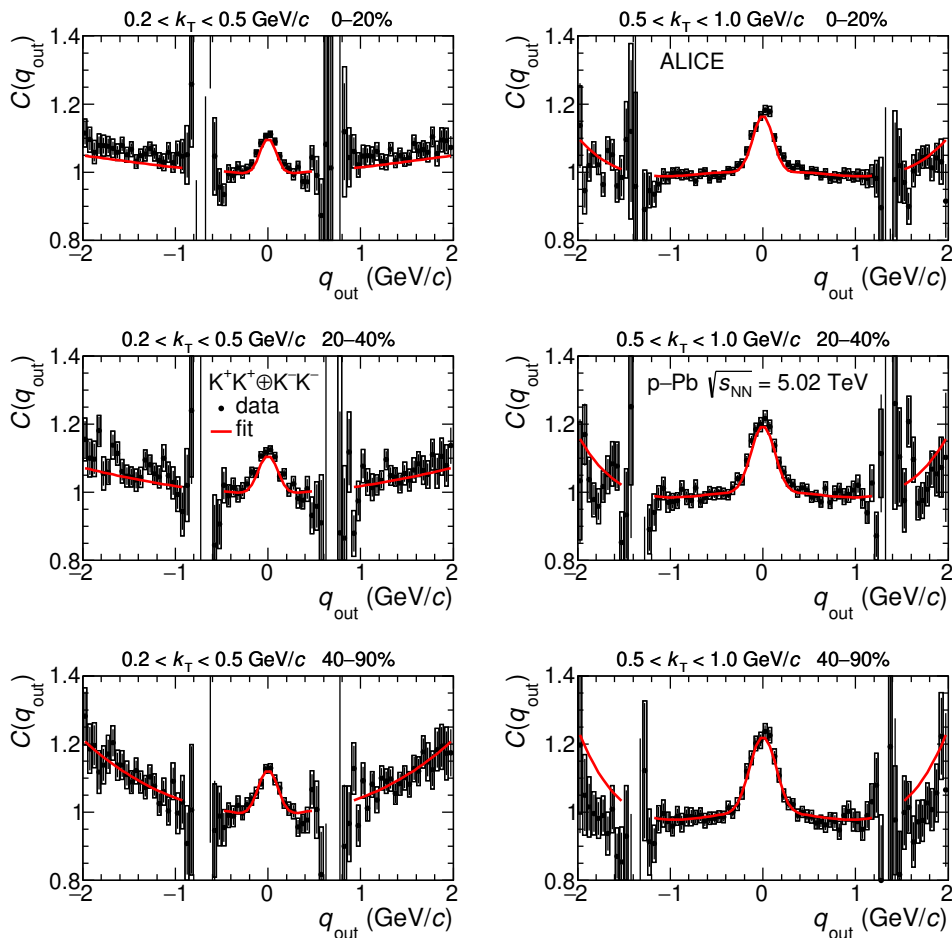


Figure 2. Projection of the 3D CF in the out direction (black full circles) in three multiplicity classes and two k_T ranges fitted (red solid lines) with eq. (3.5). Statistical (systematic) uncertainties are shown by bars (boxes). The data are integrated over the range of $|q_i| < 0.15$ GeV/c in the non-projected coordinates. Vertical lines not belonging to any marker around $|q_{out}| = 0.6$ GeV/c are very-large error bars of data points that are out of the chosen Y axis range.

Coulomb part of the two-kaon wave function integrated over the spherical Gaussian source with a fixed radius R_{inv} calculated in the PRF. The average q_{inv} in the PRF for the given “out-side-long” interval was determined during the $C(\mathbf{q})$ construction. The value of this radius was chosen to be 1.5 fm like in the 1D analysis (see section 3.1).

The CF was fitted with eq. (3.5) in the $|q_i| < 1.5$ GeV/c range. The baseline was parametrized with a fourth-order polynomial

$$D(\mathbf{q}) = 1 + a_{out}q_{out}^2 + a_{side}q_{side}^2 + a_{long}q_{long}^2 + b_{out}q_{out}^4 + b_{side}q_{side}^4 + b_{long}q_{long}^4, \quad (3.6)$$

which reasonably describes the CF outside the femtoscopic peak region. The results are shown in figures 2–4. As can be seen from the figures, the fit reproduces well the shape of the correlation peak and also captures non-femtoscopic behavior of all projections of the 3D correlation function. The areas with no data points in the q_{out} projection around ± 0.6 GeV/c and in the q_{long} projection below -0.8 (and above 0.8) GeV/c originate from

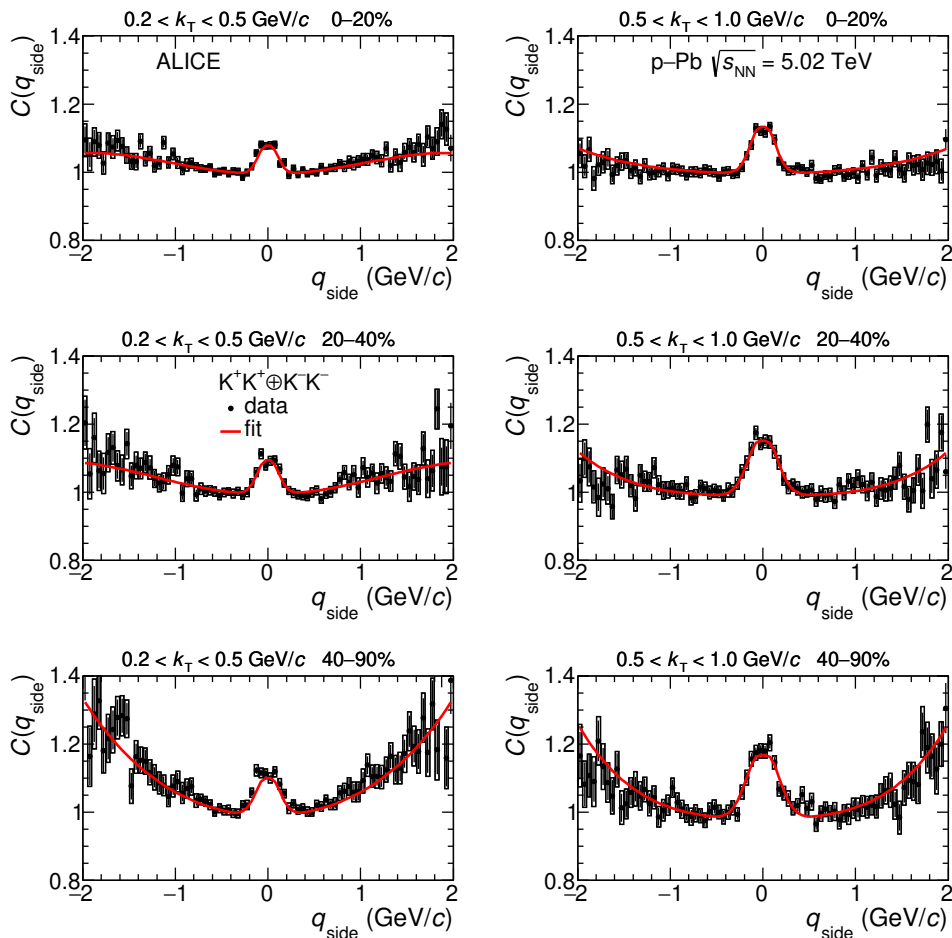


Figure 3. Projection of the 3D CF in the side direction (black full circles) in three multiplicity classes and two k_T ranges fitted (red solid lines) with eq. (3.5). Statistical (systematic) uncertainties are shown by bars (boxes). The data are integrated over the range of $|q_i| < 0.15$ GeV/c in the non-projected coordinates.

gaps in the acceptance due to the kinematical selections used in the analysis and the limited pseudorapidity acceptance of the detector, respectively [40].

4 Systematic uncertainties

The systematic uncertainties were estimated by varying the criteria used for the selection of the events, tracks, and pairs and the fit parameters. The criteria used for particle identification and pair selection were varied by up to $\pm 20\%$. The influence of the fit range was investigated by shifting the q_{inv} ($q_{out,side,long}$) upper (left and right) limit(s) by $\pm 20\%$. The range of the primary-vertex position from the center of the detector along the beam direction z for reconstructed events was varied by $\pm 10\%$.

There is also an uncertainty associated with the choice of the radius of the Coulomb interaction. By default, it was set to $r = 1.5$ fm as a result of averaging the values of the femtoscopic radii that were extracted from the data for the considered multiplicity classes and k_T ranges and varied by ± 0.5 fm.

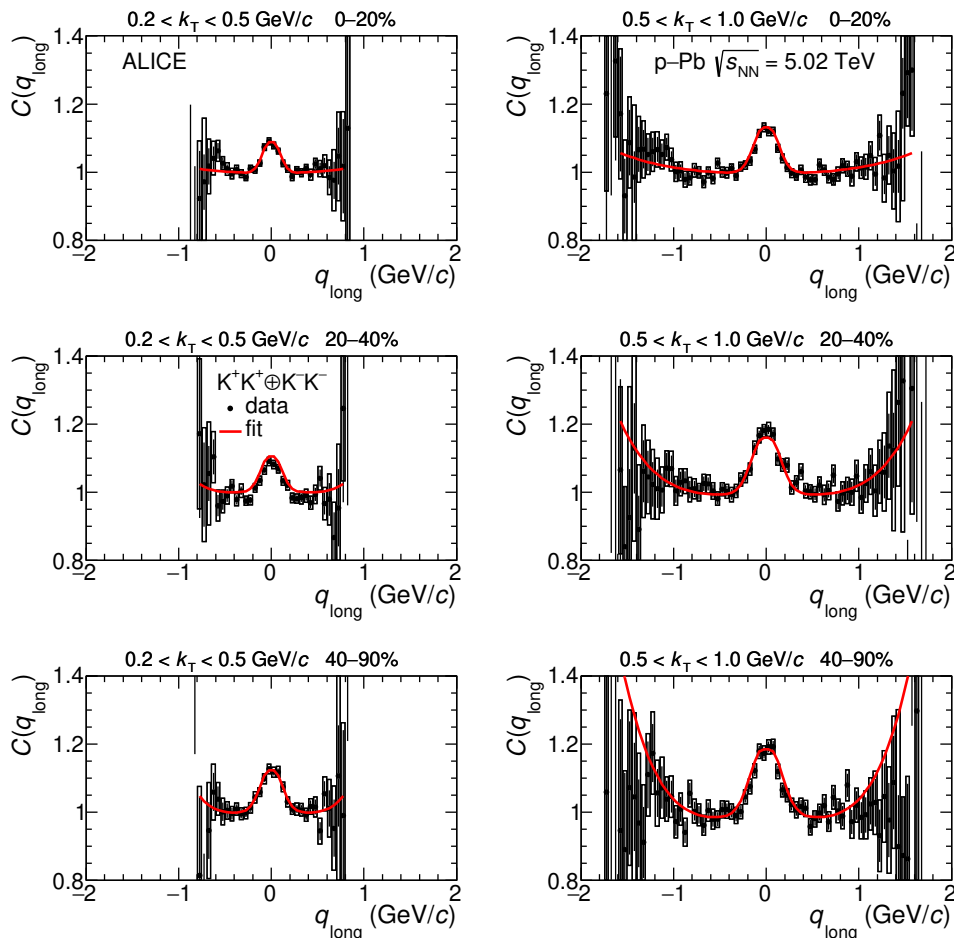


Figure 4. Projection of the 3D CF in the long direction (black full circles) in three multiplicity classes and two k_T ranges fitted (red solid lines) with eq. (3.5). Statistical (systematic) uncertainties are shown by bars (boxes). The data are integrated over the range of $|q_i| < 0.15$ GeV/c in the non-projected coordinates. Vertical lines not belonging to any marker at $|q_{\text{long}}| \gtrsim 1.0$ GeV/c are very-large error bars of data points that are out of the chosen Y axis range.

The fitting procedure requires knowledge of the non-femtoscopic background shape and magnitude. In this work, the EPOS 3 model was used for this purpose in the 1D analysis. The systematic uncertainty associated with the baseline was estimated using an alternative MC model, DPMJET, as well as the two methods based on the use of polynomials described in ref. [35]. In the 3D analysis, a flat baseline and the DPMJET model were considered as alternative baseline descriptions.

The smearing of the single-particle momenta due to momentum resolution reduces the height and increases the width of the correlation function. It was shown that this effect changes the extracted parameters by $< 1\%$ both in the 1D and in the 3D analyses, estimated as described in ref. [39] and in ref. [45], respectively.

The Barlow criterion [83] was applied to estimate a statistical significance level of the effect produced by every systematic contribution i as

$$\mathfrak{B} = \frac{|y_0 - y_{\text{var}}^i|}{\sqrt{\sigma_0^2 + \sigma_{\text{var}}^i{}^2 - 2\rho\sigma_0\sigma_{\text{var}}^i}}, \quad (4.1)$$

	R_{inv} (%)	λ (%)
DCA	0.8–2.2	1.2–11
Number of points in TPC	0.5–10	1–11
η range	0.5–10	3–21
z vertex position	0.2–10	0.3–12
Number of mixed events	0.4–3	1–11
Two-track selection	1.4–4	1.8–12
Baseline	2.5–6	0.4–4
Fit range	1–7	0.5–4
Coulomb radius	0.8–1.9	0–5

Table 4. List of contributions to the systematic uncertainty of the 1D femtoscopic radii R_{inv} and correlation strength λ in six multiplicity classes: 0–5%, 5–10%, 10–20%, 20–40%, 40–60%, and 60–80% and two pair transverse momentum k_T ranges: (0.2–0.5) and (0.5–1.0) GeV/ c . The minimum-maximum values in all multiplicity classes and k_T ranges are shown.

where σ_0 is the statistical uncertainty of the central value y_0 extracted from the analysis with the default selection criteria and fit parameters, σ_{var}^i is the statistical uncertainty of the value y_{var}^i obtained with a given variation i of particle selections and parameters of the fit, and ρ characterizes the correlation between y_0 and y_{var}^i . The variation y_{var}^i was included in the total systematic uncertainty

$$\Delta_{\text{sys}} = \sqrt{\sum_i (\Delta_{\text{sys}}^i)^2}, \tag{4.2}$$

where $\Delta_{\text{sys}}^i = |y_0 - y_{\text{var}}^i|$, if \mathfrak{B} in eq. (4.1) was larger than unity.

The contributions to the systematic uncertainty of the radii and correlation strengths are given in table 4 for the 1D analysis in six multiplicity and two k_T ranges, in table 5 for the analysis in three multiplicity and eight k_T ranges, and in table 6 for the 3D analysis. Selected according to the Barlow criterium, the main sources of systematic uncertainty on the extracted parameters are the baseline description, the single particle and pair selection criteria, and the number of events used to construct the reference distribution $B(\mathbf{q})$ in eq. (3.1).

5 Results and discussion

5.1 1D analysis results

The extracted R_{inv} and λ parameters in six multiplicity classes and two k_T ranges are depicted in figure 5. The presented results are also compared with the EPOS 3 model [84–86] with the hadronic afterburner (UrQMD cascade) [87] included, for the same collision system and energy in the same multiplicity and k_T ranges as the experimental data. In the previous work on p–Pb collisions [35], the experimental radii were compared with the EPOS 3 calculations in wider 0–20%, 20–40%, and 40–90% multiplicity classes since the available data at the time did not enable a study in finer multiplicity intervals. The EPOS 3 radii were found to agree with the data in ref. [35] within uncertainties. The present 1D analysis shows that

	R_{inv} (%)	λ (%)
DCA	0.5–13	1–19
Number of points in TPC	1–14	0–18
η range	1–13.5	2.5–13
z vertex position	0.2–14	1–20
Number of mixed events	1.4–14	2–13.5
Two-track selection	1.5–15	2–27
Baseline	2–10.5	0.5–7
Fit range	0.2–16	0.1–11
Coulomb radius	0.5–2	4.5–5.5

Table 5. List of contributions to the systematic uncertainty of the 1D femtoscopic radii R_{inv} and correlation strength λ in three multiplicity classes: 0–20%, 20–40%, and 40–90% and in eight k_T ranges: (0.2–0.3), (0.3–0.4), (0.4–0.5), (0.5–0.6), (0.6–0.7), (0.7–0.8), (0.8–1.0), and (1.0–1.3) GeV/ c . The minimum-maximum values in all multiplicity classes and k_T ranges are shown.

	R_{out} (%)	R_{side} (%)	R_{long} (%)	λ (%)
DCA	0.2–2.7	1.3–9	1–4	1–2.5
Number of points in TPC	2–9	2–5	1–5	1.5–10
η range	2–7.5	2–6	1–10	1–11
z vertex position	0.1–6.5	0.2–3.2	0.3–5.5	0.3–8.5
Number of mixed events	0–6.5	0–6	1–6	0.2–8
Two-track selection	0.2–9	0.2–3.5	0–6	0–10
Baseline	3–16	1.5–25	1–24	6–22
Fit range	1.5–9	2–5	1.5–7	1.3–4
Coulomb radius	1.2–2.1	0.8–1.9	0.8–1.8	4.8–5.2

Table 6. List of contributions to the systematic uncertainty of the 3D femtoscopic radii R_{out} , R_{side} , R_{long} and correlation strength λ in three multiplicity classes: 0–20%, 20–40%, and 40–90% and two pair transverse momentum k_T ranges: (0.2–0.5) and (0.5–1.0) GeV/ c . The minimum-maximum values in all multiplicity classes and k_T ranges are shown.

the radii are well reproduced by the EPOS 3 model calculations for the semicentral and peripheral collisions. At the same time, the model tends to underestimate R_{inv} for the 0–5% multiplicity interval. The EPOS 3 correlation strength values are about 0.65 and larger than the λ values extracted from the experimental data, which lie around 0.35. The value of the λ parameter equals unity in the case of a perfectly Gaussian spherical source with pure primary particles emitted from the source chaotically. In reality, a fraction of kaons could be emitted coherently [81, 88], and also there are kaons from K^* decays (whose decay width $\Gamma \approx$ is 50 MeV) and from other long-lived resonances [89], whose contribution decreases the λ value. A similar difference between the λ values from the data and from the EPOS 3 predictions was already observed before in ref. [35] and was explained by insufficient accounting for all contributions of kaons from various resonance decays in the model.

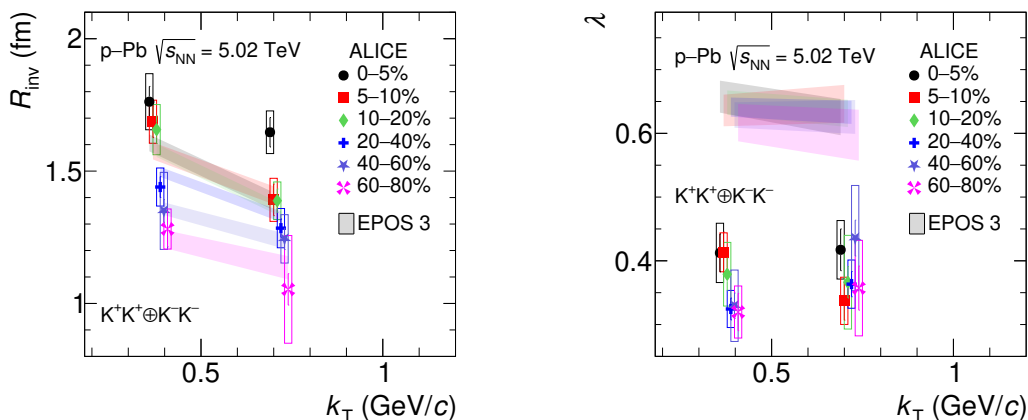


Figure 5. Experimental (symbols) $K^\pm K^\pm$ invariant radii R_{inv} (left) and correlation strengths λ (right) shown as a function of the pair transverse momentum k_T for six multiplicity classes and compared with the EPOS 3 model predictions. The width of the bands represents the statistical uncertainty of the EPOS 3 predictions. The different colors of the bands correspond to the respective centralities as given by the ALICE data. Statistical (lines) and systematic uncertainties (boxes) are shown for the data points. The points for lower multiplicity classes are slightly shifted with respect to the 0–5% multiplicity class (black symbols) in the x direction for clarity.

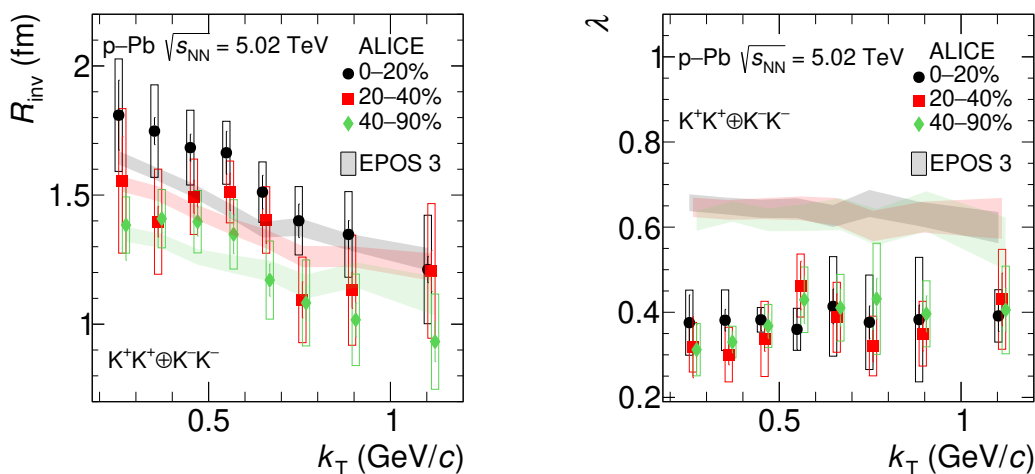


Figure 6. Experimental (symbols) $K^\pm K^\pm$ invariant radii R_{inv} (left) and correlation strengths λ (right) shown as a function of the pair transverse momentum k_T for three multiplicity classes and compared with the EPOS 3 model predictions. The width of the bands represents the statistical uncertainty of the model calculations. The different colors of the bands correspond to the respective centralities as given by the ALICE data. Statistical (lines) and systematic uncertainties (boxes) are shown for the data points. The points for lower multiplicity classes are slightly shifted with respect to the 0–20% multiplicity class (black symbols) in the x direction for clarity.

	a	b	χ^2/NDF
	low k_T		
pp&p-Pb	0.11 ± 0.12	0.49 ± 0.04	1.42
Pb-Pb	0.64 ± 0.23	0.45 ± 0.03	0.83
	high k_T		
pp&p-Pb	0.36 ± 0.19	0.32 ± 0.06	1.12
Pb-Pb	0.93 ± 0.22	0.34 ± 0.02	0.92

Table 7. Parameters of the $(a + b\langle N_{\text{ch}}^{1/3} \rangle)$ fit of the 1D radii in figure 7.

The R_{inv} and λ parameters in three multiplicity classes and eight k_T ranges are shown in figure 6, and they provide a more detailed insight into the k_T trend. The radii are well reproduced by the EPOS 3 model except for the 0–20% multiplicity class at low $k_T \lesssim 0.6$ GeV/ c where there is an indication that the model underestimates the radii extracted from the experimental data. This provides a more detailed insight into how the EPOS 3 model describes the data as compared to the previous analysis of p–Pb collisions that was performed in wider k_T ranges [35]. For the λ parameter, the discrepancy between the EPOS 3 result and the data is similar to that observed in the case of six multiplicity classes and two k_T ranges discussed above.

Figure 7 compares the femtoscopic radii extracted in this analysis as a function of the cube root of the measured charged-particle multiplicity $\langle N_{\text{ch}} \rangle^{1/3}$, at low (left) and high (right) k_T with those obtained in pp [32], p–Pb [35], and Pb–Pb [37, 58] collisions. The radii increase with N_{ch} , and the Run 2 p–Pb results agree within uncertainties with the Run 1 ones [35]. Thanks to the Pb–Pb analysis in the very peripheral centrality ranges [58], it became possible to compare the radii in p–Pb and Pb–Pb collisions at comparable multiplicities N_{ch} . The radii are equal in p–Pb and pp collisions at similar multiplicity within uncertainties. As the figure shows, the trends of the radii as a function of $\langle N_{\text{ch}} \rangle^{1/3}$ in pp and p–Pb collisions and separately in Pb–Pb collisions can be well reproduced by a first-order polynomial, supporting the so-called “scaling hypothesis” [26] that supposes the proportionality of the total multiplicity to the interferometry volume. It is also seen that the line fitting the pp and p–Pb data is shifted vertically with respect to the one fitting the Pb–Pb points, and this shift increases with increasing k_T (see table 7). The observed different offsets can be considered as an indication of different transverse flow velocities in matter created in pp (p–Pb) and Pb–Pb collisions, originating from the different initial geometric sizes [56], or the different source geometry in the final state [26]. The obtained result reinforces the conclusion made in the earlier p–Pb analysis [35] about the similarity of dynamics of the source in p–Pb and pp collisions at low multiplicities. According to the models in refs. [56, 90], this means that the expansion is not significantly stronger in p–Pb than in pp collisions.

5.2 3D analysis results

5.2.1 Radius and correlation strength

Figure 8 shows the k_T dependence of the extracted 3D kaon radii R_{out} , R_{side} , R_{long} , and correlation strength λ in the case of three multiplicity and two k_T ranges. As seen from

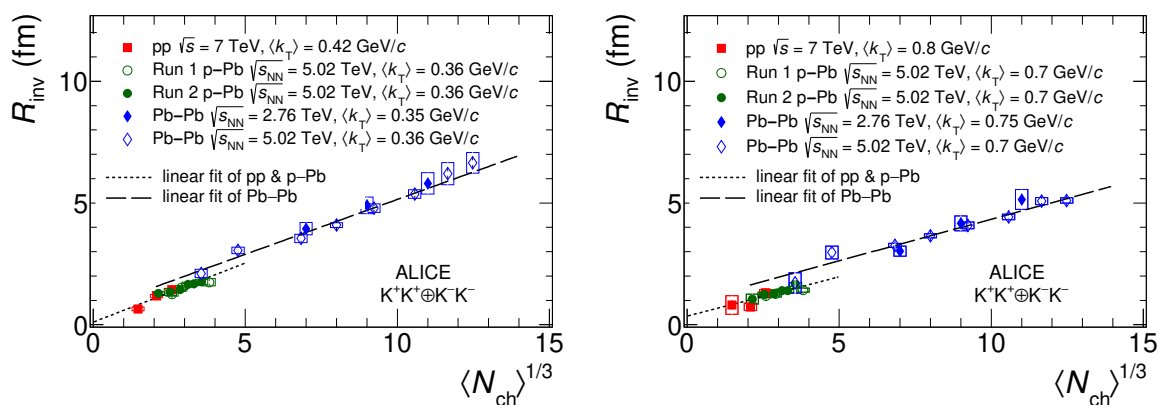


Figure 7. Femtoscopic radii extracted in the present analysis (green solid circles), as a function of the cube root of the measured charged-particle multiplicity $\langle N_{\text{ch}} \rangle^{1/3}$, at low (left) and high (right) k_T compared with published results from pp [32] (red solid squares), p-Pb [35] (green empty circles), and Pb-Pb [37, 58] (blue diamonds) collisions. Statistical (lines) and systematic uncertainties (boxes) are shown. The dotted (dashed) line shows the fit of the pp and p-Pb (Pb-Pb) data with a first-order polynomial.

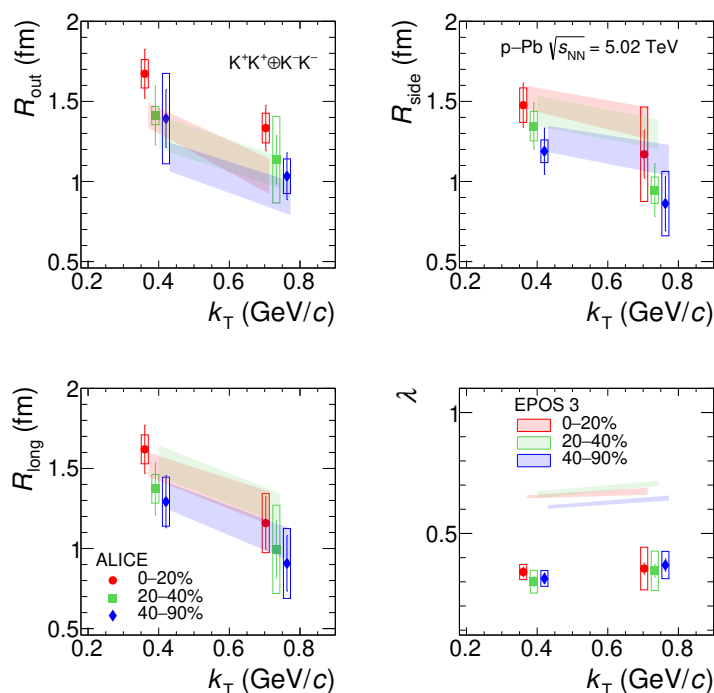


Figure 8. 3D R and λ parameters as a function of k_T in three multiplicity and two k_T classes. The experimental data (markers) are compared with the EPOS 3 model predictions shown by bands, the width of which represents the statistical uncertainty on the model calculations. Statistical (bars) and systematic (rectangles) uncertainties are shown. Points are shifted with respect to the 0–20% multiplicity class along the x axis for clarity.

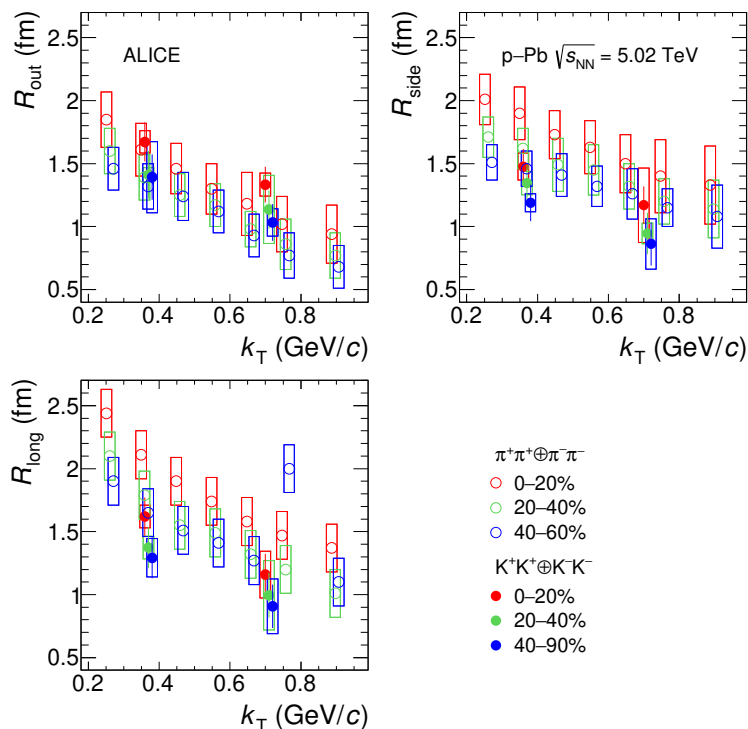


Figure 9. 3D R parameters as a function of k_T for pion (empty circles) and kaon (full circles) pairs. Statistical (bars) and systematic (rectangles) uncertainties are shown. Points are shifted with respect to the 0–20% multiplicity class along the x axis for clarity.

the figure, the extracted experimental radii decrease for more peripheral collisions and with increasing k_T within the 1.0 to 1.7 fm interval. The obtained λ values do not depend on multiplicity or k_T , are around ≈ 0.3 and equal within uncertainties to the correlation strength values extracted in the 1D analysis. The EPOS 3 radii agree with the experimental ones within uncertainties, although there is an indication that EPOS 3 underestimates the R_{out} component of the 3D radius for the most central collisions. A similar behavior was observed for $K^\pm K^\pm$ correlations in Pb–Pb collisions at $\sqrt{s_{\text{NN}}} = 5.02$ TeV [58] in comparison to the integrated hydrokinetic model [56] and for πK correlations in Pb–Pb collisions at $\sqrt{s_{\text{NN}}} = 2.76$ TeV [91] in comparison to the (3+1)D hydrodynamic model + THERMINATOR 2 [92]. Therefore, to provide a better description of the femtoscopic data, hydrodynamic models should be improved. The EPOS 3 predictions for the λ parameter do not depend on k_T and multiplicity and are larger (≈ 0.65) than the experimental ones similarly to the 1D analysis result, possibly due to the contributions of kaons from long-lived (for example, K^*) resonance decays.

Figure 9 compares the extracted 3D radii R_{out} , R_{side} , and R_{long} for pion [41] and kaon pairs as a function of k_T . The comparison demonstrates that the pion and kaon radii agree within uncertainties at the same multiplicity and k_T . Unfortunately, the quite large uncertainties of the available experimental data for pions and kaons do not allow for a fine comparison of the radii to see if they scale better with the pair transverse mass m_T or the pair transverse momentum k_T . The k_T scaling was observed in the 3D analysis of identical charged kaon correlations in Pb–Pb collisions at $\sqrt{s_{\text{NN}}} = 2.76$ TeV [45], although the hydrodynamic

scenario of nuclear collisions for the particular case of small transverse flow predicted the m_T scaling for the longitudinal radii (R_{long}) for pions and kaons [93]. The obtained k_T scaling instead was interpreted as an indication of the importance of the hadronic rescattering phase at LHC energies [48, 94, 95]. However, more experimental data are needed to clarify whether m_T or k_T scaling occurs for pions and kaons in p-Pb collisions.

5.2.2 Time of maximal emission

In this work, based on the combined fit of the kaon R_{long}^2 dependence on m_T and the pion and kaon transverse momentum spectra, the time of maximal emission [56, 57] for kaons τ_K was estimated as follows.

The first step is to perform a combined fit of pion and kaon p_T spectra using

$$E \frac{d^3N}{d^3p} \propto \exp \left[- \left(\frac{m_T}{T} + \alpha \right) \sqrt{1 - \bar{v}_T^2} \right], \quad (5.1)$$

where T is the temperature of maximal emission, α is a parameter characterizing the strength of collective flow (infinite value means zero flow, and small value means strong flow), and $\bar{v}_T = \frac{k_T}{m_T + \alpha T}$ is the transverse collective velocity. From the fit, the common effective temperature of pions and kaons T and the value of α for each particle species are extracted.

At the second step, the fit of R_{long}^2 for kaons is carried out using the formula

$$R_{\text{long}}^2(m_T) = \tau^2 \zeta^2 \left(1 + \frac{3}{2} \zeta^2 \right), \quad (5.2)$$

$$\zeta^2 = \frac{T}{m_T} \sqrt{1 - \bar{v}_T^2}. \quad (5.3)$$

When performing this fit, the temperature T is taken from the fit of the spectra. However, the α_K parameter for kaons was left unconstrained following the approach used for A-A collisions [56, 57, 59].

The τ_K parameter was also extracted in the femtoscopic identical charged kaon analyses in Pb-Pb collisions at $\sqrt{s_{\text{NN}}} = 2.76$ TeV [45] and at $\sqrt{s_{\text{NN}}} = 5.02$ TeV [58]. Unlike the mentioned Pb-Pb analyses, the available experimental data in p-Pb are limited. Therefore, in this work, a simultaneous fit of pion and kaon p_T spectra (eq. (5.1)) and kaon R_{long} (eq. (5.2)) was performed to extract the time of kaon maximal emission τ_K . Such a fitting procedure provided the stability of the extracted τ_K value. The spectra were taken from ref. [64]. In addition, since the three τ_K values extracted in the three corresponding multiplicity classes were found to agree within uncertainties, they were averaged together to obtain a single τ_K value with a smaller statistical uncertainty. The systematic uncertainties of τ_K were determined by propagating the systematic uncertainties of R_{long} .

The resulting $\tau_K = 2.7 \pm 0.25(\text{stat.}) \pm 0.15(\text{syst.})$ is shown in figure 10. It agrees within uncertainties with the value of the time of maximal emission in very peripheral Pb-Pb collisions at the same collision energy. Thus, the kaon emission duration in p-Pb collisions is comparable with that in Pb-Pb collisions at a similar multiplicity. In terms of physical interpretation, it means that the kaon emission process in p-Pb and in very peripheral Pb-Pb collisions occurs similarly over time.

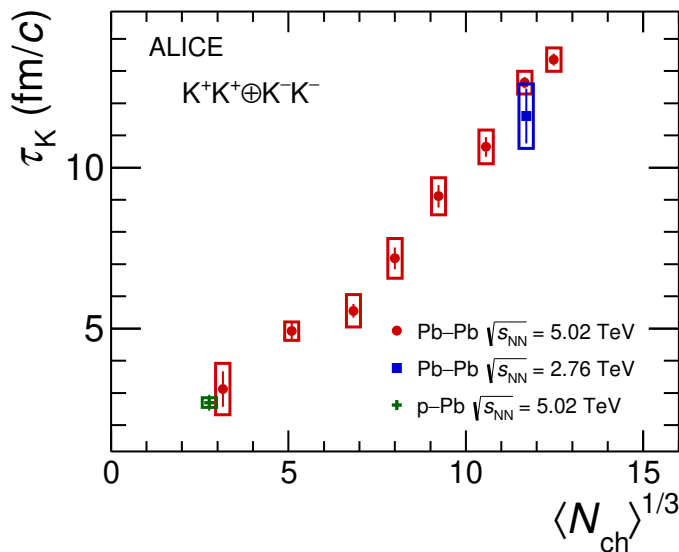


Figure 10. Time of maximal emission τ_K as a function of the cube root of the charged particle multiplicity $\langle N_{ch} \rangle^{1/3}$ in p-Pb (green symbol, this work) and Pb-Pb (red [58] and blue [45] symbols) collisions.

6 Summary

In summary, identical charged kaon pair 1D and 3D correlations were measured in p-Pb collisions at $\sqrt{s_{NN}} = 5.02$ TeV. The source radii decrease with increasing pair transverse mass and decreasing event multiplicity both in the 1D and the 3D analyses, similar to the measurements in A-A and high-multiplicity pp collisions in accordance with the hydrodynamic expansion scenario of the medium created in high-energy collisions. The comparison of the obtained results with the EPOS 3 predictions shows that this model does not describe R_{inv} for the most central events, while the description is very good for semicentral and peripheral collisions. The model describes, within uncertainties, the measured 3D radii for all the multiplicity classes and k_T ranges, although there is an indication of discrepancy between the experimental and the model R_{out} . However, in order to make a statistically significant statement for this discrepancy more experimental data are needed. The comparison of R_{inv} as a function of the multiplicity in pp, p-Pb, and Pb-Pb collisions demonstrates that pp and p-Pb points follow the same linear trend. The linear trend for the R_{inv} values in Pb-Pb collisions has a similar slope but a different offset. The gap between these two fitting lines tends to increase with increasing k_T . The same observation was done for the pion correlation analysis earlier. This result disfavors models that incorporate substantially stronger collective expansion in p-Pb collisions compared to pp collisions at similar multiplicity.

The correlation strength λ is independent of multiplicity or k_T within uncertainties. The values of the λ parameters calculated with EPOS 3 are larger than those extracted from the experimental data. The observed discrepancy could be due to the influence of long-lived resonances.

The 3D pion and kaon radii agree within uncertainties at the same multiplicity and pair transverse momentum k_T . The available experimental data do not allow concluding whether $\pi^\pm\pi^\pm$ and $K^\pm K^\pm$ radii scale with the transverse mass or the transverse momentum.

Based on the 3D analysis, the time of maximal emission τ_K was extracted for identical charged kaons in p–Pb collisions. The obtained value is equal to the value of τ_K in very peripheral Pb–Pb collisions at the same collision energy indicating the same kaon emission duration in the matter created in p–Pb and Pb–Pb collisions at similar multiplicity.

Acknowledgments

The ALICE Collaboration would like to thank all its engineers and technicians for their invaluable contributions to the construction of the experiment and the CERN accelerator teams for the outstanding performance of the LHC complex. The ALICE Collaboration gratefully acknowledges the resources and support provided by all Grid centres and the Worldwide LHC Computing Grid (WLCG) collaboration. The ALICE Collaboration acknowledges the following funding agencies for their support in building and running the ALICE detector: A.I. Alikhanyan National Science Laboratory (Yerevan Physics Institute) Foundation (ANSL), State Committee of Science and World Federation of Scientists (WFS), Armenia; Austrian Academy of Sciences, Austrian Science Fund (FWF): [M 2467-N36] and Nationalstiftung für Forschung, Technologie und Entwicklung, Austria; Ministry of Communications and High Technologies, National Nuclear Research Center, Azerbaijan; Rede Nacional de Física de Altas Energias (Renafae), Financiadora de Estudos e Projetos (Finep), Fundação de Amparo à Pesquisa do Estado de São Paulo (FAPESP) and Universidade Federal do Rio Grande do Sul (UFRGS), Brazil; Bulgarian Ministry of Education and Science, within the National Roadmap for Research Infrastructures 2020–2027 (object CERN), Bulgaria; Ministry of Education of China (MOEC), Ministry of Science & Technology of China (MSTC) and National Natural Science Foundation of China (NSFC), China; Ministry of Science and Education and Croatian Science Foundation, Croatia; Centro de Aplicaciones Tecnológicas y Desarrollo Nuclear (CEADEN), Cubaenergía, Cuba; Ministry of Education, Youth and Sports of the Czech Republic, Czech Republic; The Danish Council for Independent Research | Natural Sciences, the VILLUM FONDEN and Danish National Research Foundation (DNRF), Denmark; Helsinki Institute of Physics (HIP), Finland; Commissariat à l’Energie Atomique (CEA) and Institut National de Physique Nucléaire et de Physique des Particules (IN2P3) and Centre National de la Recherche Scientifique (CNRS), France; Bundesministerium für Forschung, Technologie und Raumfahrt (BMFTR) and GSI Helmholtzzentrum für Schwerionenforschung GmbH, Germany; General Secretariat for Research and Technology, Ministry of Education, Research and Religions, Greece; National Research, Development and Innovation Office, Hungary; Department of Atomic Energy Government of India (DAE), Department of Science and Technology, Government of India (DST), University Grants Commission, Government of India (UGC) and Council of Scientific and Industrial Research (CSIR), India; National Research and Innovation Agency – BRIN, Indonesia; Istituto Nazionale di Fisica Nucleare (INFN), Italy; Japanese Ministry of Education, Culture, Sports, Science and Technology (MEXT) and Japan Society for the Promotion of Science (JSPS) KAKENHI, Japan; Consejo Nacional de Ciencia (CONACYT) y Tecnología, through Fondo de Cooperación Interna-

cional en Ciencia y Tecnología (FONCICYT) and Dirección General de Asuntos del Personal Académico (DGAPA), Mexico; Nederlandse Organisatie voor Wetenschappelijk Onderzoek (NWO), Netherlands; The Research Council of Norway, Norway; Pontificia Universidad Católica del Perú, Peru; Ministry of Science and Higher Education, National Science Centre and WUT ID-UB, Poland; Korea Institute of Science and Technology Information and National Research Foundation of Korea (NRF), Republic of Korea; Ministry of Education and Scientific Research, Institute of Atomic Physics, Ministry of Research and Innovation and Institute of Atomic Physics and Universitatea Nationala de Stiinta si Tehnologie Politehnica Bucuresti, Romania; Ministerstvo školstva, vyzkumu, vyvoja a mladeze SR, Slovakia; National Research Foundation of South Africa, South Africa; Swedish Research Council (VR) and Knut & Alice Wallenberg Foundation (KAW), Sweden; European Organization for Nuclear Research, Switzerland; Suranaree University of Technology (SUT), National Science and Technology Development Agency (NSTDA) and National Science, Research and Innovation Fund (NSRF via PMU-B B05F650021), Thailand; Turkish Energy, Nuclear and Mineral Research Agency (TENMAK), Turkey; National Academy of Sciences of Ukraine, Ukraine; Science and Technology Facilities Council (STFC), United Kingdom; National Science Foundation of the United States of America (NSF) and United States Department of Energy, Office of Nuclear Physics (DOE NP), United States of America. In addition, individual groups or members have received support from: Czech Science Foundation (grant no. 23-07499S), Czech Republic; FORTE project, reg. no. CZ.02.01.01/00/22_008/0004632, Czech Republic, co-funded by the European Union, Czech Republic; European Research Council (grant no. 950692), European Union; ICSC – Centro Nazionale di Ricerca in High Performance Computing, Big Data and Quantum Computing, European Union – NextGenerationEU; Academy of Finland (Center of Excellence in Quark Matter) (grant nos. 346327, 346328), Finland; Deutsche Forschungsgemeinschaft (DFG, German Research Foundation) “Neutrinos and Dark Matter in Astro- and Particle Physics” (grant no. SFB 1258), Germany.

Data Availability Statement. This manuscript has associated data in a HEPData repository at: <https://www.hepdata.net/record/ins3109745>.

Code Availability Statement. This manuscript has associated code/software in a data repository. The code/software used for the analysis is publicly available on the github repository, at the links <https://github.com/alisw/AliRoot> and <https://github.com/alisw/AliPhysics/>.

Open Access. This article is distributed under the terms of the Creative Commons Attribution License ([CC-BY4.0](https://creativecommons.org/licenses/by/4.0/)), which permits any use, distribution and reproduction in any medium, provided the original author(s) and source are credited.

References

- [1] L. Evans and P. Bryant, *LHC Machine*, 2008 *JINST* **3** S08001 [INSPIRE].
- [2] CMS collaboration, *First measurement of large area jet transverse momentum spectra in heavy-ion collisions*, *JHEP* **05** (2021) 284 [arXiv:2102.13080] [INSPIRE].
- [3] ALICE collaboration, *Measurements of inclusive jet spectra in pp and central Pb–Pb collisions at $\sqrt{s_{NN}} = 5.02$ TeV*, *Phys. Rev. C* **101** (2020) 034911 [arXiv:1909.09718] [INSPIRE].
- [4] ATLAS collaboration, *Measurements of the suppression and correlations of dijets in Pb+Pb collisions at $\sqrt{s_{NN}} = 5.02$ TeV*, *Phys. Rev. C* **107** (2023) 054908 [Erratum *ibid.* **109** (2024) 029901] [arXiv:2205.00682] [INSPIRE].
- [5] ALICE collaboration, *$K^*(892)^0$ and $\phi(1020)$ meson production at high transverse momentum in pp and Pb–Pb collisions at $\sqrt{s_{NN}} = 2.76$ TeV*, *Phys. Rev. C* **95** (2017) 064606 [arXiv:1702.00555] [INSPIRE].
- [6] ALICE collaboration, *Evidence of rescattering effect in Pb–Pb collisions at the LHC through production of $K^*(892)^0$ and $\phi(1020)$ mesons*, *Phys. Lett. B* **802** (2020) 135225 [arXiv:1910.14419] [INSPIRE].
- [7] NA49 collaboration, *Ξ^- and Ξ^+ production in central Pb+Pb collisions at 158 GeV/c per nucleon*, *Phys. Lett. B* **538** (2002) 275 [hep-ex/0202037] [INSPIRE].
- [8] ALICE collaboration, *Multi-strange baryon production at mid-rapidity in Pb–Pb collisions at $\sqrt{s_{NN}} = 2.76$ TeV*, *Phys. Lett. B* **728** (2014) 216 [arXiv:1307.5543] [INSPIRE].
- [9] P. Faccioli and C. Lourenço, *The fate of quarkonia in heavy-ion collisions at LHC energies: a unified description of the sequential suppression patterns*, *Eur. Phys. J. C* **78** (2018) 731 [arXiv:1809.10488] [INSPIRE].
- [10] CMS collaboration, *Observation of Sequential Υ Suppression in Pb–Pb Collisions*, *Phys. Rev. Lett.* **109** (2012) 222301 [Erratum *ibid.* **120** (2018) 199903] [arXiv:1208.2826] [INSPIRE].
- [11] ALICE collaboration, *Υ production and nuclear modification at forward rapidity in Pb–Pb collisions at $\sqrt{s_{NN}} = 5.02$ TeV*, *Phys. Lett. B* **822** (2021) 136579 [arXiv:2011.05758] [INSPIRE].
- [12] ALICE collaboration, *Production of inclusive $\Upsilon(1S)$ and $\Upsilon(2S)$ in p–Pb collisions at $\sqrt{s_{NN}} = 5.02$ TeV*, *Phys. Lett. B* **740** (2015) 105 [arXiv:1410.2234] [INSPIRE].
- [13] CMS collaboration, *Strange hadron collectivity in pPb and PbPb collisions*, *JHEP* **05** (2023) 007 [arXiv:2205.00080] [INSPIRE].
- [14] ALICE collaboration, *Anisotropic flow and flow fluctuations of identified hadrons in Pb–Pb collisions at $\sqrt{s_{NN}} = 5.02$ TeV*, *JHEP* **05** (2023) 243 [arXiv:2206.04587] [INSPIRE].
- [15] C. Gale, S. Jeon and B. Schenke, *Hydrodynamic Modeling of Heavy-Ion Collisions*, *Int. J. Mod. Phys. A* **28** (2013) 1340011 [arXiv:1301.5893] [INSPIRE].
- [16] U. Heinz and R. Snellings, *Collective flow and viscosity in relativistic heavy-ion collisions*, *Ann. Rev. Nucl. Part. Sci.* **63** (2013) 123 [arXiv:1301.2826] [INSPIRE].
- [17] P. Romatschke and U. Romatschke, *Relativistic Fluid Dynamics In and Out of Equilibrium*, Cambridge University Press (2019) [DOI:10.1017/9781108651998] [INSPIRE].
- [18] BRAHMS collaboration, *Quark-gluon plasma and color glass condensate at RHIC? The Perspective from the BRAHMS experiment*, *Nucl. Phys. A* **757** (2005) 1 [nucl-ex/0410020] [INSPIRE].

- [19] STAR collaboration, *Experimental and theoretical challenges in the search for the quark-gluon plasma: The STAR Collaboration's critical assessment of the evidence from RHIC collisions*, *Nucl. Phys. A* **757** (2005) 102 [[nucl-ex/0501009](#)] [[INSPIRE](#)].
- [20] CMS collaboration, *Study of high- p_T charged particle suppression in PbPb compared to pp collisions at $\sqrt{s_{NN}} = 2.76$ TeV*, *Eur. Phys. J. C* **72** (2012) 1945 [[arXiv:1202.2554](#)] [[INSPIRE](#)].
- [21] ATLAS collaboration, *Measurement of the jet radius and transverse momentum dependence of inclusive jet suppression in lead-lead collisions at $\sqrt{s_{NN}} = 2.76$ TeV with the ATLAS detector*, *Phys. Lett. B* **719** (2013) 220 [[arXiv:1208.1967](#)] [[INSPIRE](#)].
- [22] ALICE collaboration, *The ALICE experiment: a journey through QCD*, *Eur. Phys. J. C* **84** (2024) 813 [[arXiv:2211.04384](#)] [[INSPIRE](#)].
- [23] G. Goldhaber, S. Goldhaber, W.-Y. Lee and A. Pais, *Influence of Bose-Einstein statistics on the anti-proton proton annihilation process*, *Phys. Rev.* **120** (1960) 300 [[INSPIRE](#)].
- [24] G.I. Kopylov, *Like particle correlations as a tool to study the multiple production mechanism*, *Phys. Lett. B* **50** (1974) 472 [[INSPIRE](#)].
- [25] R. Lednicky, *Correlation femtoscopy*, *Nucl. Phys. A* **774** (2006) 189 [[nucl-th/0510020](#)] [[INSPIRE](#)].
- [26] M.A. Lisa, S. Pratt, R. Soltz and U. Wiedemann, *Femtoscopy in Relativistic Heavy Ion Collisions: Two Decades of Progress*, *Ann. Rev. Nucl. Part. Sci.* **55** (2005) 357 [[nucl-ex/0505014](#)] [[INSPIRE](#)].
- [27] U.W. Heinz and G. Kestin, *Jozso's Legacy: Chemical and Kinetic Freeze-out in Heavy-Ion Collisions*, *Eur. Phys. J. ST* **155** (2008) 75 [[arXiv:0709.3366](#)] [[INSPIRE](#)].
- [28] S.V. Akkelin and Y.M. Sinyukov, *The HBT-interferometry of expanding sources*, *Phys. Lett. B* **356** (1995) 525 [[INSPIRE](#)].
- [29] M.G. Bowler, *Bose-Einstein Symmetrization: Coherence and Chaos: With Particular Application to e^+e^- Annihilation*, *Z. Phys. C* **29** (1985) 617 [[INSPIRE](#)].
- [30] CMS collaboration, *Measurement of Bose-Einstein Correlations in pp Collisions at $\sqrt{s} = 0.9$ and 7 TeV*, *JHEP* **05** (2011) 029 [[arXiv:1101.3518](#)] [[INSPIRE](#)].
- [31] ALICE collaboration, *$K_s^0 - K_s^0$ correlations in pp collisions at $\sqrt{s} = 7$ TeV from the LHC ALICE experiment*, *Phys. Lett. B* **717** (2012) 151 [[arXiv:1206.2056](#)] [[INSPIRE](#)].
- [32] ALICE collaboration, *Charged kaon femtosopic correlations in pp collisions at $\sqrt{s} = 7$ TeV*, *Phys. Rev. D* **87** (2013) 052016 [[arXiv:1212.5958](#)] [[INSPIRE](#)].
- [33] CMS collaboration, *Bose-Einstein correlations of charged hadrons in proton-proton collisions at $\sqrt{s} = 13$ TeV*, *JHEP* **03** (2020) 014 [[arXiv:1910.08815](#)] [[INSPIRE](#)].
- [34] ALICE collaboration, *$K_s^0 K_s^0$ and $K_s^0 K^\pm$ femtoscopy in pp collisions at $\sqrt{s} = 5.02$ and 13 TeV*, *Phys. Lett. B* **833** (2022) 137335 [[arXiv:2111.06611](#)] [[INSPIRE](#)].
- [35] ALICE collaboration, *One-dimensional charged kaon femtoscopy in p-Pb collisions at $\sqrt{s_{NN}} = 5.02$ TeV*, *Phys. Rev. C* **100** (2019) 024002 [[arXiv:1903.12310](#)] [[INSPIRE](#)].
- [36] LHCb collaboration, *Study of the Bose-Einstein correlations of same-sign pions in proton-lead collisions*, *JHEP* **09** (2023) 172 [[arXiv:2306.09755](#)] [[INSPIRE](#)].
- [37] ALICE collaboration, *One-dimensional pion, kaon, and proton femtoscopy in Pb-Pb collisions at $\sqrt{s_{NN}} = 2.76$ TeV*, *Phys. Rev. C* **92** (2015) 054908 [[arXiv:1506.07884](#)] [[INSPIRE](#)].



- [38] ALICE collaboration, *Freeze-out radii extracted from three-pion cumulants in pp, p-Pb and Pb-Pb collisions at the LHC*, *Phys. Lett. B* **739** (2014) 139 [[arXiv:1404.1194](#)] [[INSPIRE](#)].
- [39] ALICE collaboration, *Investigation of K^+K^- interactions via femtoscopy in Pb-Pb collisions at $\sqrt{s_{NN}} = 2.76$ TeV at the CERN Large Hadron Collider*, *Phys. Rev. C* **107** (2023) 054904 [[arXiv:2211.15194](#)] [[INSPIRE](#)].
- [40] ALICE collaboration, *Femtoscopy of pp collisions at $\sqrt{s} = 0.9$ and 7 TeV at the LHC with two-pion Bose-Einstein correlations*, *Phys. Rev. D* **84** (2011) 112004 [[arXiv:1101.3665](#)] [[INSPIRE](#)].
- [41] ALICE collaboration, *Two-pion femtoscopy in p-Pb collisions at $\sqrt{s_{NN}} = 5.02$ TeV*, *Phys. Rev. C* **91** (2015) 034906 [[arXiv:1502.00559](#)] [[INSPIRE](#)].
- [42] ATLAS collaboration, *Femtoscopy with identified charged pions in proton-lead collisions at $\sqrt{s_{NN}} = 5.02$ TeV with ATLAS*, *Phys. Rev. C* **96** (2017) 064908 [[arXiv:1704.01621](#)] [[INSPIRE](#)].
- [43] E802 collaboration, *Two-particle rapidity correlations from the Bose-Einstein effect in central $^{28}\text{Si}+\text{Au}$ collisions at 14.6A GeV/c and intermittency*, *Phys. Rev. C* **56** (1997) 1544 [[INSPIRE](#)].
- [44] PHENIX collaboration, *Kaon Interferometric Probes of Space-Time Evolution in Au+Au Collisions at $\sqrt{s_{NN}} = 200$ GeV*, *Phys. Rev. Lett.* **103** (2009) 142301 [[arXiv:0903.4863](#)] [[INSPIRE](#)].
- [45] ALICE collaboration, *Kaon femtoscopy in Pb-Pb collisions at $\sqrt{s_{NN}} = 2.76$ TeV*, *Phys. Rev. C* **96** (2017) 064613 [[arXiv:1709.01731](#)] [[INSPIRE](#)].
- [46] H. Beker et al., *Kaon interferometry in heavy-ion collisions at the CERN SPS*, *Z. Phys. C* **64** (1994) 209 [[INSPIRE](#)].
- [47] R.A. Soltz et al., *Constraining the initial temperature and shear viscosity in a hybrid hydrodynamic model of $\sqrt{s_{NN}} = 200$ GeV Au+Au collisions using pion spectra, elliptic flow, and femtoscopic radii*, *Phys. Rev. C* **87** (2013) 044901 [[arXiv:1208.0897](#)] [[INSPIRE](#)].
- [48] I.A. Karpenko, Y.M. Sinyukov and K. Werner, *Uniform description of bulk observables in the hydrokinetic model of A + A collisions at the BNL Relativistic Heavy Ion Collider and the CERN Large Hadron Collider*, *Phys. Rev. C* **87** (2013) 024914 [[arXiv:1204.5351](#)] [[INSPIRE](#)].
- [49] Y. Hirono and E. Shuryak, *Femtoscopic signature of strong radial flow in high-multiplicity pp collisions*, *Phys. Rev. C* **91** (2015) 054915 [[arXiv:1412.0063](#)] [[INSPIRE](#)].
- [50] V.M. Shapoval, P. Braun-Munzinger, I.A. Karpenko and Y.M. Sinyukov, *Femtoscopic scales in p + p and p+Pb collisions in view of the uncertainty principle*, *Phys. Lett. B* **725** (2013) 139 [[arXiv:1304.3815](#)] [[INSPIRE](#)].
- [51] PHENIX collaboration, *Comparison of the space-time extent of the emission source in d+Au and Au+Au collisions at $\sqrt{s_{NN}} = 200$ GeV*, *Nucl. Phys. A* **931** (2014) 1082 [[arXiv:1404.5291](#)] [[INSPIRE](#)].
- [52] P. Bożek, *Femtoscopic analysis of d-Au interactions at $\sqrt{s} = 200$ GeV*, *Phys. Rev. C* **90** (2014) 064913 [[arXiv:1408.1264](#)] [[INSPIRE](#)].
- [53] K. Werner, B. Guiot, I. Karpenko and T. Pierog, *Analysing radial flow features in p-Pb and p-p collisions at several TeV by studying identified particle production in EPOS3*, *Phys. Rev. C* **89** (2014) 064903 [[arXiv:1312.1233](#)] [[INSPIRE](#)].
- [54] T. Csorgo and B. Lorstad, *Bose-Einstein correlations for three-dimensionally expanding, cylindrically symmetric, finite systems*, *Phys. Rev. C* **54** (1996) 1390 [[hep-ph/9509213](#)] [[INSPIRE](#)].

- [55] P. Danielewicz and S. Pratt, *Analyzing correlation functions with tesseral and cartesian spherical harmonics*, *Phys. Rev. C* **75** (2007) 034907 [[nucl-th/0612076](#)] [[INSPIRE](#)].
- [56] V.M. Shapoval, M.D. Adzhymambetov and Y.M. Sinyukov, *Femtoscopy scales and particle production in the relativistic heavy ion collisions from Au+Au at 200 AGeV to Xe+Xe at 5.44 ATeV within the integrated hydrokinetic model*, *Eur. Phys. J. A* **56** (2020) 260 [[arXiv:2006.16697](#)] [[INSPIRE](#)].
- [57] Y.M. Sinyukov, V.M. Shapoval and V.Y. Naboka, *On m_T dependence of femtoscopy scales for meson and baryon pairs*, *Nucl. Phys. A* **946** (2016) 227 [[arXiv:1508.01812](#)] [[INSPIRE](#)].
- [58] ALICE collaboration, *One- and three-dimensional identical charged-kaon femtosopic correlations in Pb–Pb collisions at $\sqrt{s_{NN}} = 5.02$ TeV*, [arXiv:2601.15054](#) CERN-EP-2025-236 [[INSPIRE](#)].
- [59] V.M. Shapoval and Y.M. Sinyukov, *Kaon and pion maximal emission times extraction from the femtoscopy analysis of 5.02A TeV LHC collisions within the integrated hydrokinetic model*, *Nucl. Phys. A* **1016** (2021) 122322 [[arXiv:2107.13089](#)] [[INSPIRE](#)].
- [60] ALICE collaboration, *ALICE: Physics performance report, volume I*, *J. Phys. G* **30** (2004) 1517 [[INSPIRE](#)].
- [61] ALICE collaboration, *The ALICE experiment at the CERN LHC*, 2008 *JINST* **3** S08002 [[INSPIRE](#)].
- [62] ALICE collaboration, *Performance of the ALICE Experiment at the CERN LHC*, *Int. J. Mod. Phys. A* **29** (2014) 1430044 [[arXiv:1402.4476](#)] [[INSPIRE](#)].
- [63] ALICE collaboration, *ALICE technical design report on forward detectors: FMD, T0 and V0*, CERN-LHCC-2004-025 (2004) [[INSPIRE](#)].
- [64] ALICE collaboration, *Multiplicity Dependence of Pion, Kaon, Proton and Λ Production in p–Pb Collisions at $\sqrt{s_{NN}} = 5.02$ TeV*, *Phys. Lett. B* **728** (2014) 25 [[arXiv:1307.6796](#)] [[INSPIRE](#)].
- [65] ALICE collaboration, *Centrality dependence of particle production in p–Pb collisions at $\sqrt{s_{NN}} = 5.02$ TeV*, *Phys. Rev. C* **91** (2015) 064905 [[arXiv:1412.6828](#)] [[INSPIRE](#)].
- [66] ALICE collaboration, *ALICE technical design report of the inner tracking system (ITS)*, CERN-LHCC-99-12 (1999) [[INSPIRE](#)].
- [67] ALICE collaboration, *Alignment of the ALICE Inner Tracking System with cosmic-ray tracks*, 2010 *JINST* **5** P03003 [[arXiv:1001.0502](#)] [[INSPIRE](#)].
- [68] ALICE collaboration, *ALICE: Technical design report of the time projection chamber*, CERN-OPEN-2000-183 (2000) [[INSPIRE](#)].
- [69] J. Alme et al., *The ALICE TPC, a large 3-dimensional tracking device with fast readout for ultra-high multiplicity events*, *Nucl. Instrum. Meth. A* **622** (2010) 316 [[arXiv:1001.1950](#)] [[INSPIRE](#)].
- [70] ALICE collaboration, *ALICE technical design report of the time-of-flight system (TOF)*, CERN-LHCC-2000-012 (2000) [[INSPIRE](#)].
- [71] ALICE collaboration, *ALICE: Addendum to the technical design report of the time of flight system (TOF)*, CERN-LHCC-2002-016 (2002) [[INSPIRE](#)].
- [72] A. Akindinov et al., *Performance of the ALICE Time-Of-Flight detector at the LHC*, *Eur. Phys. J. Plus* **128** (2013) 44 [[INSPIRE](#)].
- [73] E. Cerron Zeballos et al., *A new type of resistive plate chamber: The multigap RPC*, *Nucl. Instrum. Meth. A* **374** (1996) 132 [[INSPIRE](#)].

- [74] ALICE collaboration, *Centrality Dependence of Charged Particle Production at Large Transverse Momentum in Pb–Pb Collisions at $\sqrt{s_{\text{NN}}} = 2.76$ TeV*, *Phys. Lett. B* **720** (2013) 52 [[arXiv:1208.2711](#)] [[INSPIRE](#)].
- [75] ALICE collaboration, *Pseudorapidity Density of Charged Particles in p–Pb Collisions at $\sqrt{s_{\text{NN}}} = 5.02$ TeV*, *Phys. Rev. Lett.* **110** (2013) 032301 [[arXiv:1210.3615](#)] [[INSPIRE](#)].
- [76] S. Roesler, R. Engel and J. Ranft, *The Monte Carlo event generator DPMJET-III*, in the proceedings of the *International Conference on Advanced Monte Carlo for Radiation Physics, Particle Transport Simulation and Applications (MC 2000)*, Lisbon, Portugal, October 23–26 (2000) [[DOI:10.1007/978-3-642-18211-2_166](#)] [[hep-ph/0012252](#)] [[INSPIRE](#)].
- [77] R. Brun et al., *GEANT Detector Description and Simulation Tool*, CERN-W5013 (1994) [[DOI:10.17181/CERN.MUHF.DMJ1](#)] [[INSPIRE](#)].
- [78] ALICE collaboration, *Λ K femtoscopy in Pb–Pb collisions at $\sqrt{s_{\text{NN}}} = 2.76$ TeV*, *Phys. Rev. C* **103** (2021) 055201 [[arXiv:2005.11124](#)] [[INSPIRE](#)].
- [79] NPLQCD collaboration, *K^+K^+ scattering length from lattice QCD*, *Phys. Rev. D* **77** (2008) 094507 [[arXiv:0709.1169](#)] [[INSPIRE](#)].
- [80] Y. Sinyukov et al., *Coulomb corrections for interferometry analysis of expanding hadron systems*, *Phys. Lett. B* **432** (1998) 248 [[INSPIRE](#)].
- [81] ALICE collaboration, *Two- and three-pion quantum statistics correlations in Pb–Pb collisions at $\sqrt{s_{\text{NN}}} = 2.76$ TeV at the CERN Large Hadron Collider*, *Phys. Rev. C* **89** (2014) 024911 [[arXiv:1310.7808](#)] [[INSPIRE](#)].
- [82] M.G. Bowler, *Coulomb corrections to Bose-Einstein correlations have been greatly exaggerated*, *Phys. Lett. B* **270** (1991) 69 [[INSPIRE](#)].
- [83] R. Barlow, *Systematic errors: Facts and fictions*, in the proceedings of the *Conference on Advanced Statistical Techniques in Particle Physics*, Durham, U.K., March 18–22 (2002) [[hep-ex/0207026](#)] [[INSPIRE](#)].
- [84] K. Werner et al., *Event-by-Event Simulation of the Three-Dimensional Hydrodynamic Evolution from Flux Tube Initial Conditions in Ultrarelativistic Heavy Ion Collisions*, *Phys. Rev. C* **82** (2010) 044904 [[arXiv:1004.0805](#)] [[INSPIRE](#)].
- [85] K. Werner, K. Mikhailov, I. Karpenko and T. Pierog, *Bose-Einstein Correlations in a Fluid Dynamical Scenario for Proton-Proton Scattering at 7 TeV*, [arXiv:1104.2405](#) [[INSPIRE](#)].
- [86] K. Werner et al., *Evidence for hydrodynamic evolution in proton-proton scattering at 900 GeV*, *Phys. Rev. C* **83** (2011) 044915 [[arXiv:1010.0400](#)] [[INSPIRE](#)].
- [87] A.G. Knospe et al., *Hadronic resonance production and interaction in partonic and hadronic matter in the EPOS3 model with and without the hadronic afterburner UrQMD*, *Phys. Rev. C* **93** (2016) 014911 [[arXiv:1509.07895](#)] [[INSPIRE](#)].
- [88] S.V. Akkelin, R. Lednicky and Y.M. Sinyukov, *Correlation search for coherent pion emission in heavy ion collisions*, *Phys. Rev. C* **65** (2002) 064904 [[nucl-th/0107015](#)] [[INSPIRE](#)].
- [89] U.A. Wiedemann and U.W. Heinz, *Resonance contributions to HBT correlation radii*, *Phys. Rev. C* **56** (1997) 3265 [[nucl-th/9611031](#)] [[INSPIRE](#)].
- [90] P. Bożek and W. Broniowski, *Size of the emission source and collectivity in ultra-relativistic p–Pb collisions*, *Phys. Lett. B* **720** (2013) 250 [[arXiv:1301.3314](#)] [[INSPIRE](#)].
- [91] ALICE collaboration, *Pion-kaon femtoscopy and the lifetime of the hadronic phase in Pb–Pb collisions at $\sqrt{s_{\text{NN}}} = 2.76$ TeV*, *Phys. Lett. B* **813** (2021) 136030 [[arXiv:2007.08315](#)] [[INSPIRE](#)].

- [92] A. Kisiel, *Pion-kaon femtoscopy in Pb–Pb collisions at $\sqrt{s_{\text{NN}}} = 2.76$ TeV modeled in (3+1)D hydrodynamics coupled to Therminator 2 and the effect of delayed kaon emission*, *Phys. Rev. C* **98** (2018) 044909 [[arXiv:1804.06781](#)] [[INSPIRE](#)].
- [93] A.N. Makhlin and Y.M. Sinyukov, *The hydrodynamics of hadron matter under pion interferometric microscope*, *Z. Phys. C* **39** (1988) 69 [[INSPIRE](#)].
- [94] PHENIX collaboration, *Systematic study of charged-pion and kaon femtoscopy in Au + Au collisions at $\sqrt{s_{\text{NN}}} = 200$ GeV*, *Phys. Rev. C* **92** (2015) 034914 [[arXiv:1504.05168](#)] [[INSPIRE](#)].
- [95] I.A. Karpenko and Y.M. Sinyukov, *Kaon and pion femtoscopy at the highest energies available at the BNL Relativistic Heavy Ion Collider (RHIC) in a hydrokinetic model*, *Phys. Rev. C* **81** (2010) 054903 [[arXiv:1004.1565](#)] [[INSPIRE](#)].

The ALICE collaboration

S. Acharya ¹²⁷, A. Agarwal¹³⁵, G. Aglieri Rinella ³², L. Aglietta ²⁴, M. Agnello ²⁹,
N. Agrawal ²⁵, Z. Ahammed ¹³⁵, S. Ahmad ¹⁵, S.U. Ahn ⁷¹, I. Ahuja ³⁶, A. Akindinov ¹⁴⁰,
V. Akishina ³⁸, M. Al-Turany ⁹⁸, D. Aleksandrov ¹⁴⁰, B. Alessandro ⁵⁶, H.M. Alfanda ⁶,
R. Alfaro Molina ⁶⁷, B. Ali ¹⁵, A. Alici ^{25,†}, N. Alizadehvandchali ¹¹⁶, A. Alkin ¹⁰⁴,
J. Alme ²⁰, G. Alocco ^{24,52}, T. Alt ⁶⁴, A.R. Altamura ⁵⁰, I. Altsybeev ⁹⁶, J.R. Alvarado ⁴⁴,
C. Andrei ⁴⁵, N. Andreou ¹¹⁵, A. Andronic ¹²⁶, E. Andronov ¹⁴⁰, V. Anguelov ⁹⁵,
F. Antinori ⁵⁴, P. Antonioli ⁵¹, N. Apadula ⁷⁴, L. Aphecetche ¹⁰³, H. Appelshäuser ⁶⁴,
C. Arata ⁷³, S. Arcelli ²⁵, R. Arnaldi ⁵⁶, J.G.M.C.A. Arneiro ¹¹⁰, I.C. Arsene ¹⁹,
M. Arslandok ¹³⁸, A. Augustinus ³², R. Averbeck ⁹⁸, D. Averyanov ¹⁴⁰, M.D. Azmi ¹⁵,
H. Baba¹²⁴, A. Badalà ⁵³, J. Bae ¹⁰⁴, Y.W. Baek ⁴⁰, X. Bai ¹²⁰, R. Bailhache ⁶⁴,
Y. Bailung ⁴⁸, R. Bala ⁹², A. Balbino ²⁹, A. Baldisseri ¹³⁰, B. Balis ², Z. Bano ⁹²,
V. Barbasova ³⁶, F. Barile ³¹, L. Barioglio ⁵⁶, M. Barlou ⁷⁹, B. Barman ⁴¹,
G.G. Barnaföldi ⁴⁶, L.S. Barnby ¹¹⁵, E. Barreau ¹⁰³, V. Barret ¹²⁷, L. Barreto ¹¹⁰,
C. Bartels ¹¹⁹, K. Barth ³², E. Bartsch ⁶⁴, N. Bastid ¹²⁷, S. Basu ^{75,†}, G. Batigne ¹⁰³,
D. Battistini ⁹⁶, B. Batyunya ¹⁴¹, D. Bauri⁴⁷, J.L. Bazo Alba ¹⁰², I.G. Bearden ⁸⁴,
C. Beattie ¹³⁸, P. Becht ⁹⁸, D. Behera ⁴⁸, I. Belikov ¹²⁹, A.D.C. Bell Hechavarria ¹²⁶,
F. Bellini ²⁵, R. Bellwied ¹¹⁶, S. Belokurova ¹⁴⁰, L.G.E. Beltran ¹⁰⁹, Y.A.V. Beltran ⁴⁴,
G. Bencedi ⁴⁶, A. Bensaoula¹¹⁶, S. Beole ²⁴, Y. Berdnikov ¹⁴⁰, A. Berdnikova ⁹⁵,
L. Bergmann ⁹⁵, M.G. Besoiu ⁶³, L. Betev ³², P.P. Bhaduri ¹³⁵, A. Bhasin ⁹²,
B. Bhattacharjee ⁴¹, L. Bianchi ²⁴, J. Bielčák ³⁴, J. Bielčiková ⁸⁷, A.P. Bigot ¹²⁹,
A. Bilandžić ⁹⁶, G. Biro ⁴⁶, S. Biswas ⁴, N. Bize ¹⁰³, J.T. Blair ¹⁰⁸, D. Blau ¹⁴⁰,
M.B. Blidaru ⁹⁸, N. Bluhme ³⁸, C. Blume ⁶⁴, G. Boca ^{21,55}, F. Bock ⁸⁸, T. Bodova ²⁰,
J. Bok ¹⁶, L. Boldizsár ⁴⁶, M. Bombara ³⁶, P.M. Bond ³², G. Bonomi ^{55,134}, H. Borel ¹³⁰,
A. Borissov ¹⁴⁰, A.G. Borquez Carcamo ⁹⁵, E. Botta ²⁴, Y.E.M. Bouziani ⁶⁴, L. Bratrud ⁶⁴,
P. Braun-Munzinger ⁹⁸, M. Bregant ¹¹⁰, M. Broz ³⁴, G.E. Bruno ^{31,97}, V.D. Buchakchiev ³⁵,
M.D. Buckland ⁸⁶, D. Budnikov ¹⁴⁰, H. Buesching ⁶⁴, S. Bufalino ²⁹, P. Buhler ⁷⁶,
N. Burmasov ¹⁴⁰, Z. Buthelezi ^{68,123}, A. Bylinkin ²⁰, S.A. Bysiak¹⁰⁷, J.C. Cabanillas Noris ¹⁰⁹,
M.F.T. Cabrera ¹¹⁶, M. Cai ⁶, H. Caines ¹³⁸, A. Caliva ²⁸, E. Calvo Villar ¹⁰²,
J.M.M. Camacho ¹⁰⁹, P. Camerini ²³, F.D.M. Canedo ¹¹⁰, S.L. Cantway ¹³⁸, M. Carabas ¹¹³,
A.A. Carballo ³², F. Carnesecchi ³², R. Caron ¹²⁸, L.A.D. Carvalho ¹¹⁰,
J. Castillo Castellanos ¹³⁰, M. Castoldi ³², F. Catalano ³², S. Cattaruzzi ²³, R. Cerri ²⁴,
I. Chakaberia ⁷⁴, P. Chakraborty ¹³⁶, S. Chandra ¹³⁵, S. Chapeland ³², M. Chartier ¹¹⁹,
S. Chattopadhyay¹³⁵, S. Chattopadhyay ¹³⁵, S. Chattopadhyay ¹⁰⁰, M. Chen ³⁹, T. Cheng ⁶,
C. Cheshkov ¹²⁸, V. Chibante Barroso ³², D.D. Chinellato ⁷⁶, E.S. Chizzali ^{96,a}, J. Cho ⁵⁸,
S. Cho ⁵⁸, P. Chochula ³², Z.A. Chochulska ^{136,b}, P. Christakoglou ⁸⁵, C.H. Christensen ⁸⁴,
P. Christiansen ⁷⁵, T. Chujo ¹²⁵, M. Ciaccio ²⁹, C. Cicalo ⁵², M.R. Ciupek⁹⁸, G. Clai^{51,c},
F. Colamaria ⁵⁰, J.S. Colburn¹⁰¹, D. Colella ³¹, A. Colelli ³¹, M. Colocci ²⁵, M. Concas ³²,
G. Conesa Balbastre ⁷³, Z. Conesa Del Valle ¹³¹, G. Contin ²³, J.G. Contreras ³⁴,
M.L. Coquet ¹⁰³, P. Cortese ^{56,133}, M.R. Cosentino ¹¹², F. Costa ³², S. Costanza ^{21,55},
C. Cot ¹³¹, P. Crochet ¹²⁷, M.M. Czarnynoga¹³⁶, A. Dainese ⁵⁴, M.C. Danisch ⁹⁵, A. Danu ⁶³,
P. Das ⁸¹, S. Das ⁴, A.R. Dash ¹²⁶, S. Dash ⁴⁷, A. De Caro ²⁸, G. De Cataldo ⁵⁰,
J. De Cuveland ³⁸, A. De Falco ²², D. De Gruttola ²⁸, N. De Marco ⁵⁶, C. De Martin ²³,

S. De Pasquale [ID](#)²⁸, R. Deb [ID](#)¹³⁴, R. Del Grande [ID](#)⁹⁶, L. Dello Stritto [ID](#)^{28,32}, W. Deng [ID](#)⁶, K.C. Devereaux¹⁸, P. Dhankher [ID](#)¹⁸, D. Di Bari [ID](#)³¹, A. Di Mauro [ID](#)³², B. Di Ruzza [ID](#)^{50,132,†}, B. Diab [ID](#)¹³⁰, R.A. Diaz [ID](#)^{7,141}, T. Dietel [ID](#)¹¹⁴, Y. Ding [ID](#)⁶, J. Ditzel [ID](#)⁶⁴, R. Divià [ID](#)³², Ø. Djuvsland²⁰, U. Dmitrieva [ID](#)¹⁴⁰, A. Dobrin [ID](#)⁶³, B. Dönigus [ID](#)⁶⁴, J.M. Dubinski [ID](#)¹³⁶, A. Dubla [ID](#)⁹⁸, P. Dupieux [ID](#)¹²⁷, N. Dzalaiova¹³, T.M. Eder [ID](#)¹²⁶, R.J. Ehlers [ID](#)⁷⁴, F. Eisenhut [ID](#)⁶⁴, R. Ejima [ID](#)⁹³, D. Elia [ID](#)⁵⁰, B. Erazmus [ID](#)¹⁰³, F. Ercolessi [ID](#)²⁵, B. Espagnon [ID](#)¹³¹, G. Eulisse [ID](#)³², D. Evans [ID](#)¹⁰¹, S. Evdokimov [ID](#)¹⁴⁰, L. Fabbietti [ID](#)⁹⁶, M. Faggin [ID](#)²³, J. Faivre [ID](#)⁷³, F. Fan [ID](#)⁶, W. Fan [ID](#)⁷⁴, T. Fang [ID](#)⁶, A. Fantoni [ID](#)⁴⁹, M. Fasel [ID](#)⁸⁸, A. Feliciello [ID](#)⁵⁶, G. Feofilov [ID](#)¹⁴⁰, A. Fernández Téllez [ID](#)⁴⁴, L. Ferrandi [ID](#)¹¹⁰, M.B. Ferrer [ID](#)³², A. Ferrero [ID](#)¹³⁰, C. Ferrero [ID](#)^{56,d}, A. Ferretti [ID](#)²⁴, V.J.G. Feuillard [ID](#)⁹⁵, D. Finogeev [ID](#)¹⁴⁰, F.M. Fionda [ID](#)⁵², E. Flatland³², F. Flor [ID](#)^{116,138}, A.N. Flores [ID](#)¹⁰⁸, S. Foertsch [ID](#)⁶⁸, I. Fokin [ID](#)⁹⁵, S. Fokin [ID](#)¹⁴⁰, U. Follo [ID](#)^{56,d}, E. Fragiaco [ID](#)⁵⁷, E. Frajna [ID](#)⁴⁶, U. Fuchs [ID](#)³², N. Funicello [ID](#)²⁸, C. Furget [ID](#)⁷³, A. Furs [ID](#)¹⁴⁰, T. Fusayasu [ID](#)⁹⁹, J.J. Gaardhøje [ID](#)⁸⁴, M. Gagliardi [ID](#)²⁴, A.M. Gago [ID](#)¹⁰², T. Gahlaut [ID](#)⁴⁷, C.D. Galvan [ID](#)¹⁰⁹, S. Gami [ID](#)⁸¹, D.R. Gangadharan [ID](#)¹¹⁶, P. Ganoti [ID](#)⁷⁹, C. Garabatos [ID](#)⁹⁸, J.M. Garcia [ID](#)⁴⁴, T. García Chávez [ID](#)⁴⁴, E. Garcia-Solis [ID](#)⁹, C. Gargiulo [ID](#)³², P. Gasik [ID](#)⁹⁸, A. Gautam [ID](#)¹¹⁸, M.B. Gay Ducati [ID](#)⁶⁶, M. Germain [ID](#)¹⁰³, R.A. Gernhaeuser [ID](#)⁹⁶, C. Ghosh¹³⁵, M. Giacalone [ID](#)⁵¹, G. Gioachin [ID](#)²⁹, S.K. Giri [ID](#)¹³⁵, P. Giubellino [ID](#)^{56,98}, P. Giubilato [ID](#)²⁷, A.M.C. Glaenger [ID](#)¹³⁰, P. Glässel [ID](#)⁹⁵, E. Glimos [ID](#)¹²², D.J.Q. Goh⁷⁷, V. Gonzalez [ID](#)¹³⁷, P. Gordeev [ID](#)¹⁴⁰, M. Gorgon [ID](#)², K. Goswami [ID](#)⁴⁸, S. Gotovac [ID](#)³³, V. Grabski [ID](#)⁶⁷, L.K. Graczykowski [ID](#)¹³⁶, E. Grecka [ID](#)⁸⁷, A. Grelli [ID](#)⁵⁹, C. Grigoras [ID](#)³², V. Grigoriev [ID](#)¹⁴⁰, S. Grigoryan [ID](#)^{1,141}, F. Grosa [ID](#)³², J.F. Grosse-Oetringhaus [ID](#)³², R. Grosso [ID](#)⁹⁸, D. Grund [ID](#)³⁴, N.A. Grunwald [ID](#)⁹⁵, G.G. Guardiano [ID](#)¹¹¹, R. Guernane [ID](#)⁷³, M. Guillaud [ID](#)¹⁰³, K. Gulbrandsen [ID](#)⁸⁴, J.K. Gumprecht [ID](#)⁷⁶, T. Gündem [ID](#)⁶⁴, T. Gunji [ID](#)¹²⁴, W. Guo [ID](#)⁶, A. Gupta [ID](#)⁹², R. Gupta [ID](#)⁹², R. Gupta [ID](#)⁴⁸, K. Gwizdział [ID](#)¹³⁶, L. Gyulai [ID](#)⁴⁶, C. Hadjidakis [ID](#)¹³¹, F.U. Haider [ID](#)⁹², S. Haidlova [ID](#)³⁴, M. Haldar⁴, H. Hamagaki [ID](#)⁷⁷, Y. Han [ID](#)¹³⁹, B.G. Hanley [ID](#)¹³⁷, R. Hannigan [ID](#)¹⁰⁸, J. Hansen [ID](#)⁷⁵, M.R. Haque [ID](#)⁹⁸, J.W. Harris [ID](#)¹³⁸, A. Harton [ID](#)⁹, M.V. Hartung [ID](#)⁶⁴, H. Hassan [ID](#)¹¹⁷, D. Hatzifotiadou [ID](#)⁵¹, P. Hauer [ID](#)⁴², L.B. Havener [ID](#)¹³⁸, E. Hellbär [ID](#)³², H. Helstrup [ID](#)³⁷, M. Hemmer [ID](#)⁶⁴, T. Herman [ID](#)³⁴, S.G. Hernandez¹¹⁶, G. Herrera Corral [ID](#)⁸, S. Herrmann [ID](#)¹²⁸, K.F. Hetland [ID](#)³⁷, B. Heybeck [ID](#)⁶⁴, H. Hillemanns [ID](#)³², B. Hippolyte [ID](#)¹²⁹, I.P.M. Hobus [ID](#)⁸⁵, F.W. Hoffmann [ID](#)⁷⁰, B. Hofman [ID](#)⁵⁹, G.H. Hong [ID](#)¹³⁹, A. Horzyk [ID](#)², Y. Hou [ID](#)⁶, P. Hristov [ID](#)³², P. Huhn⁶⁴, L.M. Huhta [ID](#)¹¹⁷, T.J. Humanic [ID](#)⁸⁹, V. Humlova [ID](#)³⁴, A. Hutson [ID](#)¹¹⁶, D. Hutter [ID](#)³⁸, M.C. Hwang [ID](#)¹⁸, R. Ilkaev¹⁴⁰, M. Inaba [ID](#)¹²⁵, G.M. Innocenti [ID](#)³², M. Ippolitov [ID](#)¹⁴⁰, A. Isakov [ID](#)⁸⁵, T. Isidori [ID](#)¹¹⁸, M.S. Islam [ID](#)¹⁰⁰, S. Iurchenko [ID](#)¹⁴⁰, M. Ivanov¹³, M. Ivanov [ID](#)⁹⁸, V. Ivanov [ID](#)¹⁴⁰, K.E. Iversen [ID](#)⁷⁵, M. Jablonski [ID](#)², B. Jacak [ID](#)^{18,74}, N. Jacazio [ID](#)²⁵, P.M. Jacobs [ID](#)⁷⁴, S. Jadlovská¹⁰⁶, J. Jadlovsky¹⁰⁶, S. Jaelani [ID](#)⁸³, C. Jahnke [ID](#)¹¹⁰, M.J. Jakubowska [ID](#)¹³⁶, D.M. Janik [ID](#)³⁴, M.A. Janik [ID](#)¹³⁶, T. Janson⁷⁰, S. Ji [ID](#)¹⁶, S. Jia [ID](#)⁸⁴, T. Jiang [ID](#)¹⁰, A.A.P. Jimenez [ID](#)⁶⁵, F. Jonas [ID](#)⁷⁴, D.M. Jones [ID](#)¹¹⁹, J.M. Jowett [ID](#)^{32,98}, J. Jung [ID](#)⁶⁴, M. Jung [ID](#)⁶⁴, A. Junique [ID](#)³², A. Jusko [ID](#)¹⁰¹, J. Kaewjai¹⁰⁵, P. Kalinak [ID](#)⁶⁰, A. Kalweit [ID](#)³², A. Karasu Uysal [ID](#)⁷², D. Karatovic [ID](#)⁹⁰, N. Karatzenis¹⁰¹, O. Karavichev [ID](#)¹⁴⁰, T. Karavicheva [ID](#)¹⁴⁰, E. Karpechev [ID](#)¹⁴⁰, M.J. Karwowska [ID](#)^{32,136}, U. Keschull [ID](#)⁷⁰, M. Keil [ID](#)³², B. Ketzer [ID](#)⁴², J. Keul [ID](#)⁶⁴, S.S. Khade [ID](#)⁴⁸, A.M. Khan [ID](#)¹²⁰, S. Khan [ID](#)¹⁵, A. Khanzadeev [ID](#)¹⁴⁰, Y. Kharlov [ID](#)¹⁴⁰, A. Khatun [ID](#)¹¹⁸, A. Khuntia [ID](#)³⁴, Z. Khuranova [ID](#)⁶⁴, B. Kileng [ID](#)³⁷, B. Kim [ID](#)¹⁰⁴, C. Kim [ID](#)¹⁶, D.J. Kim [ID](#)¹¹⁷, E.J. Kim [ID](#)⁶⁹, J. Kim [ID](#)¹³⁹, J. Kim [ID](#)⁵⁸, J. Kim [ID](#)^{32,69}, M. Kim [ID](#)¹⁸, S. Kim [ID](#)¹⁷, T. Kim [ID](#)¹³⁹,

K. Kimura [ID](#)⁹³, A. Kirkova [ID](#)³⁵, S. Kirsch [ID](#)⁶⁴, I. Kisel [ID](#)³⁸, S. Kiselev [ID](#)¹⁴⁰, A. Kisiel [ID](#)¹³⁶,
 J.P. Kitowski [ID](#)², J.L. Klay [ID](#)⁵, J. Klein [ID](#)³², S. Klein [ID](#)⁷⁴, C. Klein-Bösing [ID](#)¹²⁶, M. Kleiner [ID](#)⁶⁴,
 T. Klemenz [ID](#)⁹⁶, A. Kluge [ID](#)³², C. Kobdaj [ID](#)¹⁰⁵, R. Kohara [ID](#)¹²⁴, T. Kollegger [ID](#)⁹⁸, A. Kondratyev [ID](#)¹⁴¹,
 N. Kondratyeva [ID](#)¹⁴⁰, J. König [ID](#)⁶⁴, S.A. Konigstorfer [ID](#)⁹⁶, P.J. Konopka [ID](#)³², G. Kornakov [ID](#)¹³⁶,
 M. Korwieser [ID](#)⁹⁶, S.D. Koryciak [ID](#)², C. Koster [ID](#)⁸⁵, A. Kotliarov [ID](#)⁸⁷, N. Kovacic [ID](#)⁹⁰,
 V. Kovalenko [ID](#)¹⁴⁰, M. Kowalski [ID](#)¹⁰⁷, V. Kozhuharov [ID](#)³⁵, G. Kozlov [ID](#)³⁸, I. Králik [ID](#)⁶⁰,
 A. Kravčáková [ID](#)³⁶, L. Krcaľ [ID](#)^{32,38}, M. Krivda [ID](#)^{60,101}, F. Krizek [ID](#)⁸⁷, K. Krizkova Gajdosova [ID](#)³²,
 C. Krug [ID](#)⁶⁶, M. Krüger [ID](#)⁶⁴, E. Kryshen [ID](#)¹⁴⁰, V. Kučera [ID](#)⁵⁸, C. Kuhn [ID](#)¹²⁹, P.G. Kuijjer [ID](#)⁸⁵,
 T. Kumaoka [ID](#)¹²⁵, D. Kumar [ID](#)¹³⁵, L. Kumar [ID](#)⁹¹, N. Kumar [ID](#)⁹¹, S. Kumar [ID](#)⁵⁰, S. Kundu [ID](#)³²,
 P. Kurashvili [ID](#)⁸⁰, A. Kurepin [ID](#)¹⁴⁰, A.B. Kurepin [ID](#)¹⁴⁰, A. Kuryakin [ID](#)¹⁴⁰, S. Kushpil [ID](#)⁸⁷,
 V. Kuskov [ID](#)¹⁴⁰, M. Kutyla [ID](#)¹³⁶, A. Kuznetsov [ID](#)¹⁴¹, M.J. Kweon [ID](#)⁵⁸, Y. Kwon [ID](#)¹³⁹,
 S.L. La Pointe [ID](#)³⁸, P. La Rocca [ID](#)²⁶, A. Lakrathok [ID](#)¹⁰⁵, M. Lamanna [ID](#)³², A.R. Landou [ID](#)⁷³,
 R. Langoy [ID](#)¹²¹, P. Larionov [ID](#)³², E. Laudi [ID](#)³², L. Lautner [ID](#)^{32,96}, R.A.N. Laveaga [ID](#)¹⁰⁹,
 R. Lavicka [ID](#)⁷⁶, R. Lea [ID](#)^{55,134}, H. Lee [ID](#)¹⁰⁴, I. Legrand [ID](#)⁴⁵, G. Legras [ID](#)¹²⁶, J. Lehrbach [ID](#)³⁸,
 A.M. Lejeune [ID](#)³⁴, T.M. Lelek [ID](#)², R.C. Lemmon [ID](#)^{86,†}, I. León Monzón [ID](#)¹⁰⁹, M.M. Lesch [ID](#)⁹⁶,
 P. Lévai [ID](#)⁴⁶, M. Li⁶, P. Li¹⁰, X. Li¹⁰, B.E. Liang-Gilman [ID](#)¹⁸, J. Lien [ID](#)¹²¹, R. Lietava [ID](#)¹⁰¹,
 I. Likmeta [ID](#)¹¹⁶, B. Lim [ID](#)²⁴, S.H. Lim [ID](#)¹⁶, V. Lindenstruth [ID](#)³⁸, C. Lippmann [ID](#)⁹⁸, D.H. Liu [ID](#)⁶,
 J. Liu [ID](#)¹¹⁹, G.S.S. Liveraro [ID](#)¹¹¹, I.M. Lofnes [ID](#)²⁰, C. Loizides [ID](#)⁸⁸, S. Lokos [ID](#)¹⁰⁷, J. Lömker [ID](#)⁵⁹,
 X. Lopez [ID](#)¹²⁷, E. López Torres [ID](#)⁷, C. Lotteau [ID](#)¹²⁸, P. Lu [ID](#)^{98,120}, Z. Lu [ID](#)¹⁰, F.V. Lugo [ID](#)⁶⁷,
 J.R. Luhder [ID](#)¹²⁶, M. Lunardon [ID](#)²⁷, G. Luparello [ID](#)⁵⁷, Y.G. Ma [ID](#)³⁹, M. Mager [ID](#)³², M. Mahlein [ID](#)⁹⁶,
 A. Maire [ID](#)¹²⁹, E. Majerz [ID](#)², M.V. Makariev [ID](#)³⁵, M. Malaev [ID](#)¹⁴⁰, G. Malfattore [ID](#)²⁵,
 N.M. Malik [ID](#)⁹², S.K. Malik [ID](#)⁹², L. Malinina [ID](#)^{141,†}, D. Mallick [ID](#)¹³¹, N. Mallick [ID](#)⁴⁸,
 G. Mandaglio [ID](#)^{30,53}, S.K. Mandal [ID](#)⁸⁰, A. Manea [ID](#)⁶³, V. Manko [ID](#)¹⁴⁰, F. Manso [ID](#)¹²⁷,
 V. Manzari [ID](#)⁵⁰, Y. Mao [ID](#)⁶, R.W. Marcjan [ID](#)², G.V. Margagliotti [ID](#)²³, A. Margotti [ID](#)⁵¹, A. Marín [ID](#)⁹⁸,
 C. Markert [ID](#)¹⁰⁸, C.F.B. Marquez³¹, P. Martinengo [ID](#)³², M.I. Martínez [ID](#)⁴⁴, G. Martínez García [ID](#)¹⁰³,
 M.P.P. Martins [ID](#)¹¹⁰, S. Masciocchi [ID](#)⁹⁸, M. Masera [ID](#)²⁴, A. Masoni [ID](#)⁵², L. Massacrier [ID](#)¹³¹,
 O. Massen [ID](#)⁵⁹, A. Mastroserio [ID](#)^{50,132}, O. Matonoha [ID](#)⁷⁵, S. Mattiazzo [ID](#)²⁷, A. Matyja [ID](#)¹⁰⁷,
 F. Mazzaschi [ID](#)^{24,32}, M. Mazzilli [ID](#)¹¹⁶, Y. Melikyan [ID](#)⁴³, M. Melo [ID](#)¹¹⁰, A. Menchaca-Rocha [ID](#)⁶⁷,
 J.E.M. Mendez [ID](#)⁶⁵, E. Meninno [ID](#)⁷⁶, A.S. Menon [ID](#)¹¹⁶, M.W. Menzel^{32,95}, M. Meres [ID](#)¹³, Y. Miake¹²⁵,
 L. Micheletti [ID](#)³², D. Mihai¹¹³, D.L. Mihaylov [ID](#)⁹⁶, A.U. Mikalsen [ID](#)²⁰, K. Mikhaylov [ID](#)^{140,141},
 N. Minafra [ID](#)¹¹⁸, D. Miśkowiec [ID](#)⁹⁸, A. Modak [ID](#)¹³⁴, B. Mohanty [ID](#)⁸¹, M. Mohisin Khan [ID](#)^{15,e},
 M.A. Molander [ID](#)⁴³, S. Monira [ID](#)¹³⁶, C. Mordasini [ID](#)¹¹⁷, D.A. Moreira De Godoy [ID](#)¹²⁶,
 I. Morozov [ID](#)¹⁴⁰, A. Morsch [ID](#)³², T. Mrnjavac [ID](#)³², V. Muccifora [ID](#)⁴⁹, S. Muhuri [ID](#)¹³⁵,
 J.D. Mulligan [ID](#)⁷⁴, A. Mulliri [ID](#)²², M.G. Munhoz [ID](#)¹¹⁰, R.H. Munzer [ID](#)⁶⁴, H. Murakami [ID](#)¹²⁴,
 S. Murray [ID](#)¹¹⁴, L. Musa [ID](#)³², J. Musinsky [ID](#)⁶⁰, J.W. Myrcha [ID](#)¹³⁶, B. Naik [ID](#)¹²³, A.I. Nambrath [ID](#)¹⁸,
 B.K. Nandi [ID](#)⁴⁷, R. Nania [ID](#)⁵¹, E. Nappi [ID](#)⁵⁰, A.F. Nassirpour [ID](#)¹⁷, V. Nastase¹¹³, A. Nath [ID](#)⁹⁵,
 S. Nath¹³⁵, C. Nattrass [ID](#)¹²², M.N. Naydenov [ID](#)³⁵, A. Neagu¹⁹, A. Negru¹¹³, E. Nekrasova¹⁴⁰,
 L. Nellen [ID](#)⁶⁵, R. Nepeivoda [ID](#)⁷⁵, S. Nese [ID](#)¹⁹, N. Nicassio [ID](#)³¹, B.S. Nielsen [ID](#)⁸⁴, E.G. Nielsen [ID](#)⁸⁴,
 S. Nikolaev [ID](#)¹⁴⁰, S. Nikulin [ID](#)¹⁴⁰, V. Nikulin [ID](#)¹⁴⁰, F. Noferini [ID](#)⁵¹, S. Noh [ID](#)¹², P. Nomokonov [ID](#)¹⁴¹,
 J. Norman [ID](#)¹¹⁹, N. Novitzky [ID](#)⁸⁸, P. Nowakowski [ID](#)¹³⁶, A. Nyanin [ID](#)¹⁴⁰, J. Nystrand [ID](#)²⁰,
 M. Ogino [ID](#)⁷⁷, S. Oh [ID](#)¹⁷, A. Ohlson [ID](#)⁷⁵, V.A. Okorokov [ID](#)¹⁴⁰, J. Oleniacz [ID](#)¹³⁶, A. Onnerstad [ID](#)¹¹⁷,
 C. Oppedisano [ID](#)⁵⁶, A. Ortiz Velasquez [ID](#)⁶⁵, J. Otwinowski [ID](#)¹⁰⁷, M. Oya⁹³, K. Oyama [ID](#)⁷⁷,
 Y. Pachmayer [ID](#)⁹⁵, S. Padhan [ID](#)⁴⁷, D. Pagano [ID](#)^{55,134}, G. Paic [ID](#)⁶⁵, S. Paisano-Guzmán [ID](#)⁴⁴,

A. Palasciano [ID](#)⁵⁰, I. Panasenکو [ID](#)⁷⁵, S. Panebianco [ID](#)¹³⁰, C. Pantouvakis [ID](#)²⁷, H. Park [ID](#)¹²⁵,
 H. Park [ID](#)¹⁰⁴, J. Park [ID](#)¹²⁵, T.Y. Park [ID](#)¹³⁹, J.E. Parkkila [ID](#)³², Y. Patley [ID](#)⁴⁷, R.N. Patra [ID](#)⁵⁰,
 B. Paul [ID](#)¹³⁵, H. Pei [ID](#)⁶, T. Peitzmann [ID](#)⁵⁹, X. Peng [ID](#)¹¹, M. Pennisi [ID](#)²⁴, S. Perciballi [ID](#)²⁴,
 D. Peresunko [ID](#)¹⁴⁰, G.M. Perez [ID](#)⁷, Y. Pestov [ID](#)¹⁴⁰, M.T. Petersen [ID](#)⁸⁴, V. Petrov [ID](#)¹⁴⁰, M. Petrovici [ID](#)⁴⁵,
 S. Piano [ID](#)⁵⁷, M. Pikna [ID](#)¹³, P. Pillot [ID](#)¹⁰³, O. Pinazza [ID](#)^{32,51}, L. Pinsky [ID](#)¹¹⁶, C. Pinto [ID](#)⁹⁶,
 S. Pisano [ID](#)⁴⁹, M. Planinic [ID](#)⁹⁰, D.K. Plociennik [ID](#)², M.G. Poghosyan [ID](#)⁸⁸, B. Polichtchouk [ID](#)¹⁴⁰,
 S. Politano [ID](#)²⁹, N. Poljak [ID](#)⁹⁰, A. Pop [ID](#)⁴⁵, S. Porteboeuf-Houssais [ID](#)¹²⁷, V. Pozdniakov [ID](#)^{141,†},
 I.Y. Pozos [ID](#)⁴⁴, K.K. Pradhan [ID](#)⁴⁸, S. Prasad [ID](#)⁴⁸, S.K. Prasad [ID](#)⁴, R. Preghenella [ID](#)⁵¹, F. Prino [ID](#)⁵⁶,
 C.A. Pruneau [ID](#)¹³⁷, I. Pshenichnov [ID](#)¹⁴⁰, M. Puccio [ID](#)³², S. Pucillo [ID](#)²⁴, M. Płoskoń [ID](#)⁷⁴, S. Qiu [ID](#)⁸⁵,
 L. Quaglia [ID](#)²⁴, A.M.K. Radhakrishnan [ID](#)⁴⁸, S. Ragoni [ID](#)¹⁴, A. Rai [ID](#)¹³⁸, A. Rakotozafindrabe [ID](#)¹³⁰,
 L. Ramello [ID](#)^{56,133}, F. Rami [ID](#)¹²⁹, C.O. Ramírez-Álvarez [ID](#)⁴⁴, M. Rasa [ID](#)²⁶, S.S. Räsänen [ID](#)⁴³,
 R. Rath [ID](#)⁵¹, M.P. Rauch [ID](#)²⁰, I. Ravasenga [ID](#)³², K.F. Read [ID](#)^{88,122}, C. Reckziegel [ID](#)¹¹²,
 A.R. Redelbach [ID](#)³⁸, K. Redlich [ID](#)^{80,f}, C.A. Reetz [ID](#)⁹⁸, H.D. Regules-Medel [ID](#)⁴⁴, A. Rehman [ID](#)²⁰,
 F. Reidt [ID](#)³², H.A. Reme-Ness [ID](#)³⁷, K. Reygiers [ID](#)⁹⁵, A. Riabov [ID](#)¹⁴⁰, V. Riabov [ID](#)¹⁴⁰, R. Ricci [ID](#)²⁸,
 M. Richter [ID](#)²⁰, A.A. Riedel [ID](#)⁹⁶, W. Riegler [ID](#)³², A.G. Riffero [ID](#)²⁴, M. Rignanese [ID](#)²⁷, C. Ripoli [ID](#)²⁸,
 C. Ristea [ID](#)⁶³, M.V. Rodriguez [ID](#)³², M. Rodríguez Cahuantzi [ID](#)⁴⁴, S.A. Rodríguez Ramírez [ID](#)⁴⁴,
 R. Rogalev [ID](#)¹⁴⁰, E. Rogochaya [ID](#)¹⁴¹, T.S. Rogoschinski [ID](#)⁶⁴, D. Rohr [ID](#)³², D. Röhrich [ID](#)²⁰,
 S. Rojas Torres [ID](#)³⁴, P.S. Rokita [ID](#)¹³⁶, G. Romanenko [ID](#)²⁵, F. Ronchetti [ID](#)³², E.D. Rosas [ID](#)⁶⁵,
 K. Roslon [ID](#)¹³⁶, A. Rossi [ID](#)⁵⁴, A. Roy [ID](#)⁴⁸, S. Roy [ID](#)⁴⁷, N. Rubini [ID](#)^{25,51}, J.A. Rudolph [ID](#)⁸⁵,
 D. Ruggiano [ID](#)¹³⁶, R. Rui [ID](#)²³, P.G. Russek [ID](#)², R. Russo [ID](#)⁸⁵, A. Rustamov [ID](#)⁸², E. Ryabinkin [ID](#)¹⁴⁰,
 Y. Ryabov [ID](#)¹⁴⁰, A. Rybicki [ID](#)¹⁰⁷, J. Ryu [ID](#)¹⁶, W. Rzesza [ID](#)¹³⁶, K. Røed [ID](#)¹⁹, B. Sabiu [ID](#)⁵¹,
 S. Sadovsky [ID](#)¹⁴⁰, J. Saetre [ID](#)²⁰, K. Šafařík [ID](#)^{34,†}, S. Saha [ID](#)⁸¹, B. Sahoo [ID](#)⁴⁸, R. Sahoo [ID](#)⁴⁸,
 S. Sahoo [ID](#)⁶¹, D. Sahu [ID](#)⁴⁸, P.K. Sahu [ID](#)⁶¹, J. Saini [ID](#)¹³⁵, K. Sajdakova [ID](#)³⁶, S. Sakai [ID](#)¹²⁵,
 M.P. Salvan [ID](#)⁹⁸, S. Sambyal [ID](#)⁹², D. Samitz [ID](#)⁷⁶, I. Sanna [ID](#)^{32,96}, T.B. Saramela [ID](#)¹¹⁰, D. Sarkar [ID](#)⁸⁴,
 P. Sarma [ID](#)⁴¹, V. Sarritzu [ID](#)²², V.M. Sarti [ID](#)⁹⁶, M.H.P. Sas [ID](#)³², S. Sawan [ID](#)⁸¹, E. Scapparone [ID](#)⁵¹,
 J. Schambach [ID](#)⁸⁸, H.S. Scheid [ID](#)⁶⁴, C. Schiaua [ID](#)⁴⁵, R. Schicker [ID](#)⁹⁵, F. Schlepper [ID](#)⁹⁵, A. Schmah [ID](#)⁹⁸,
 C. Schmidt [ID](#)⁹⁸, H.R. Schmidt [ID](#)⁹⁴, M. Schmidt [ID](#)⁹⁴, M.O. Schmidt [ID](#)³², N.V. Schmidt [ID](#)⁸⁸,
 A.R. Schmier [ID](#)¹²², R. Schotter [ID](#)^{76,129}, A. Schröter [ID](#)³⁸, J. Schukraft [ID](#)³², K. Schweda [ID](#)⁹⁸,
 G. Scioli [ID](#)²⁵, E. Scomparin [ID](#)⁵⁶, J.E. Seger [ID](#)¹⁴, Y. Sekiguchi [ID](#)¹²⁴, D. Sekihata [ID](#)¹²⁴, M. Selina [ID](#)⁸⁵,
 I. Selyuzhenkov [ID](#)⁹⁸, S. Senyukov [ID](#)¹²⁹, J.J. Seo [ID](#)⁹⁵, D. Serebryakov [ID](#)¹⁴⁰, L. Serkin [ID](#)^{65,g},
 L. Šerkšnyte [ID](#)⁹⁶, A. Sevcenco [ID](#)⁶³, T.J. Shaba [ID](#)⁶⁸, A. Shabetai [ID](#)¹⁰³, R. Shahoyan [ID](#)³²,
 A. Shangaraev [ID](#)¹⁴⁰, B. Sharma [ID](#)⁹², D. Sharma [ID](#)⁴⁷, H. Sharma [ID](#)⁵⁴, M. Sharma [ID](#)⁹², S. Sharma [ID](#)⁷⁷,
 S. Sharma [ID](#)⁹², U. Sharma [ID](#)⁹², A. Shatat [ID](#)¹³¹, O. Sheibani [ID](#)¹¹⁶, K. Shigaki [ID](#)⁹³, M. Shimomura [ID](#)⁷⁸,
 J. Shin [ID](#)¹², S. Shirinkin [ID](#)¹⁴⁰, Q. Shou [ID](#)³⁹, Y. Sibiriak [ID](#)¹⁴⁰, S. Siddhanta [ID](#)⁵², T. Siemiarczuk [ID](#)⁸⁰,
 T.F. Silva [ID](#)¹¹⁰, D. Silvermyr [ID](#)⁷⁵, T. Simantathammakul [ID](#)¹⁰⁵, R. Simeonov [ID](#)³⁵, B. Singh [ID](#)⁹²,
 B. Singh [ID](#)⁹⁶, K. Singh [ID](#)⁴⁸, R. Singh [ID](#)⁸¹, R. Singh [ID](#)⁹², R. Singh [ID](#)⁹⁸, S. Singh [ID](#)¹⁵, V.K. Singh [ID](#)¹³⁵,
 V. Singhal [ID](#)¹³⁵, T. Sinha [ID](#)¹⁰⁰, B. Sitar [ID](#)¹³, M. Sitta [ID](#)^{56,133}, T.B. Skaali [ID](#)¹⁹, G. Skorodumovs [ID](#)⁹⁵,
 N. Smirnov [ID](#)¹³⁸, R.J.M. Snellings [ID](#)⁵⁹, E.H. Solheim [ID](#)¹⁹, J. Song [ID](#)¹⁶, C. Sonnabend [ID](#)^{32,98},
 J.M. Sonneveld [ID](#)⁸⁵, F. Soramel [ID](#)²⁷, A.B. Soto-Hernandez [ID](#)⁸⁹, R. Spijkers [ID](#)⁸⁵, I. Sputowska [ID](#)¹⁰⁷,
 J. Staa [ID](#)⁷⁵, J. Stachel [ID](#)⁹⁵, I. Stan [ID](#)⁶³, P.J. Steffanic [ID](#)¹²², T. Stellhorn [ID](#)¹²⁶, S.F. Stiefelmaier [ID](#)⁹⁵,
 D. Stocco [ID](#)¹⁰³, I. Storehaug [ID](#)¹⁹, N.J. Strangmann [ID](#)⁶⁴, P. Stratmann [ID](#)¹²⁶, S. Strazzi [ID](#)²⁵,
 A. Sturniolo [ID](#)^{30,53}, C.P. Stylianidis [ID](#)⁸⁵, A.A.P. Suaide [ID](#)¹¹⁰, C. Suire [ID](#)¹³¹, M. Sukhanov [ID](#)¹⁴⁰,
 M. Suljic [ID](#)³², R. Sultanov [ID](#)¹⁴⁰, V. Sumberia [ID](#)⁹², S. Sumowidagdo [ID](#)⁸³, S. Swain [ID](#)⁶¹, L.H. Tabares [ID](#)⁷,

S.F. Taghavi ⁹⁶, G. Taillepied ⁹⁸, J. Takahashi ¹¹¹, G.J. Tambave ⁸¹, S. Tang ⁶, Z. Tang ¹²⁰, J.D. Tapia Takaki ¹¹⁸, N. Tapus ¹¹³, L.A. Tarasovicova ³⁶, M.G. Tarzila ⁴⁵, G.F. Tassielli ³¹, A. Tauro ³², A. Tavira García ¹³¹, G. Tejada Muñoz ⁴⁴, L. Terlizzi ²⁴, C. Terrevoli ⁵⁰, S. Thakur ⁴, D. Thomas ¹⁰⁸, A. Tikhonov ¹⁴⁰, N. Tiltmann ^{32,126}, A.R. Timmins ¹¹⁶, M. Tkacik¹⁰⁶, T. Tkacik ¹⁰⁶, A. Toia ⁶⁴, R. Tokumoto⁹³, S. Tomassini ²⁵, K. Tomohiro⁹³, Q. Tong ⁶, N. Topilskaya ¹⁴⁰, M. Toppi ⁴⁹, V.V. Torres ¹⁰³, A.G. Torres Ramos ³¹, A. Trifiró ^{30,53}, T. Triloki ⁹⁷, A.S. Triolo ^{30,32,53}, S. Tripathy ³², T. Tripathy ⁴⁷, S. Trogolo ²⁴, V. Trubnikov ³, W.H. Trzaska ¹¹⁷, T.P. Trzcinski ¹³⁶, C. Tsolanta¹⁹, R. Tu³⁹, A. Tumkin ¹⁴⁰, R. Turrisi ⁵⁴, T.S. Tveter ¹⁹, K. Ullaland ²⁰, B. Ulukutlu ⁹⁶, S. Upadhyaya ¹⁰⁷, A. Uras ¹²⁸, M. Urioni ¹³⁴, G.L. Usai ²², M. Vala ³⁶, N. Valle ⁵⁵, L.V.R. Van Doremalen⁵⁹, M. Van Leeuwen ⁸⁵, C.A. Van Veen ⁹⁵, R.J.G. Van Weelden ⁸⁵, P. Vande Vyvre ³², D. Varga ⁴⁶, Z. Varga ⁴⁶, P. Vargas Torres ⁶⁵, M. Vasileiou ⁷⁹, A. Vasiliev ^{140,†}, O. Vázquez Doce ⁴⁹, O. Vazquez Rueda ¹¹⁶, V. Vechernin ¹⁴⁰, E. Vercellin ²⁴, S. Vergara Limón⁴⁴, R. Verma ⁴⁷, L. Vermunt ⁹⁸, R. Vértesi ⁴⁶, M. Verweij ⁵⁹, L. Vickovic³³, Z. Vilakazi¹²³, O. Villalobos Baillie ¹⁰¹, A. Villani ²³, A. Vinogradov ¹⁴⁰, T. Virgili ²⁸, M.M.O. Virta ¹¹⁷, A. Vodopyanov ¹⁴¹, B. Volkel ³², M.A. Völkl ⁹⁵, S.A. Voloshin ¹³⁷, G. Volpe ³¹, B. Von Haller ³², I. Vorobyev ³², N. Vozniuk ¹⁴⁰, J. Vrláková ³⁶, J. Wan³⁹, C. Wang ³⁹, D. Wang ³⁹, Y. Wang ³⁹, Y. Wang ⁶, Z. Wang ³⁹, A. Wegrzynek ³², F. Weiglhofer ³⁸, S.C. Wenzel ³², J.P. Wessels ¹²⁶, J. Wiechula ⁶⁴, J. Wikne ¹⁹, G. Wilk ⁸⁰, J. Wilkinson ⁹⁸, G.A. Willems ¹²⁶, B. Windelband ⁹⁵, M. Winn ¹³⁰, J.R. Wright ¹⁰⁸, W. Wu³⁹, Y. Wu ¹²⁰, Z. Xiong¹²⁰, L. Xu ⁶, R. Xu ⁶, A. Yadav ⁴², A.K. Yadav ¹³⁵, Y. Yamaguchi ⁹³, S. Yang ²⁰, S. Yano ⁹³, E.R. Yeats ¹⁸, Z. Yin ⁶, I.-K. Yoo ¹⁶, J.H. Yoon ⁵⁸, H. Yu ¹², S. Yuan²⁰, A. Yuncu ⁹⁵, V. Zaccolo ²³, C. Zampolli ³², F. Zanone ⁹⁵, N. Zardoshti ³², A. Zarochentsev ¹⁴⁰, P. Závada ⁶², N. Zaviyalov¹⁴⁰, M. Zhalov ¹⁴⁰, B. Zhang ^{6,95}, C. Zhang ¹³⁰, L. Zhang ³⁹, M. Zhang ^{6,127}, M. Zhang ⁶, S. Zhang ³⁹, X. Zhang ⁶, Y. Zhang¹²⁰, Z. Zhang ⁶, M. Zhao ¹⁰, V. Zhrebchevskii ¹⁴⁰, Y. Zhi¹⁰, D. Zhou ⁶, Y. Zhou ⁸⁴, J. Zhu ^{6,54}, S. Zhu¹²⁰, Y. Zhu⁶, S.C. Zugravel ⁵⁶, N. Zurlo ^{55,134}

¹ A.I. Alikhanyan National Science Laboratory (Yerevan Physics Institute) Foundation, Yerevan, Armenia

² AGH University of Krakow, Cracow, Poland

³ Bogolyubov Institute for Theoretical Physics, National Academy of Sciences of Ukraine, Kyiv, Ukraine

⁴ Bose Institute, Department of Physics and Centre for Astroparticle Physics and Space Science (CAPSS), Kolkata, India

⁵ California Polytechnic State University, San Luis Obispo, California, U.S.A.

⁶ Central China Normal University, Wuhan, China

⁷ Centro de Aplicaciones Tecnológicas y Desarrollo Nuclear (CEADEN), Havana, Cuba

⁸ Centro de Investigación y de Estudios Avanzados (CINVESTAV), Mexico City and Mérida, Mexico

⁹ Chicago State University, Chicago, Illinois, U.S.A.

¹⁰ China Nuclear Data Center, China Institute of Atomic Energy, Beijing, China

¹¹ China University of Geosciences, Wuhan, China

¹² Chungbuk National University, Cheongju, Republic of Korea

¹³ Comenius University Bratislava, Faculty of Mathematics, Physics and Informatics, Bratislava, Slovak Republic

¹⁴ Creighton University, Omaha, Nebraska, U.S.A.

¹⁵ Department of Physics, Aligarh Muslim University, Aligarh, India

¹⁶ Department of Physics, Pusan National University, Pusan, Republic of Korea

¹⁷ Department of Physics, Sejong University, Seoul, Republic of Korea

- ¹⁸ *Department of Physics, University of California, Berkeley, California, U.S.A.*
- ¹⁹ *Department of Physics, University of Oslo, Oslo, Norway*
- ²⁰ *Department of Physics and Technology, University of Bergen, Bergen, Norway*
- ²¹ *Dipartimento di Fisica, Università di Pavia, Pavia, Italy*
- ²² *Dipartimento di Fisica dell'Università and Sezione INFN, Cagliari, Italy*
- ²³ *Dipartimento di Fisica dell'Università and Sezione INFN, Trieste, Italy*
- ²⁴ *Dipartimento di Fisica dell'Università and Sezione INFN, Turin, Italy*
- ²⁵ *Dipartimento di Fisica e Astronomia dell'Università and Sezione INFN, Bologna, Italy*
- ²⁶ *Dipartimento di Fisica e Astronomia dell'Università and Sezione INFN, Catania, Italy*
- ²⁷ *Dipartimento di Fisica e Astronomia dell'Università and Sezione INFN, Padova, Italy*
- ²⁸ *Dipartimento di Fisica 'E.R. Caianiello' dell'Università and Gruppo Collegato INFN, Salerno, Italy*
- ²⁹ *Dipartimento DISAT del Politecnico and Sezione INFN, Turin, Italy*
- ³⁰ *Dipartimento di Scienze MIFT, Università di Messina, Messina, Italy*
- ³¹ *Dipartimento Interateneo di Fisica 'M. Merlin' and Sezione INFN, Bari, Italy*
- ³² *European Organization for Nuclear Research (CERN), Geneva, Switzerland*
- ³³ *Faculty of Electrical Engineering, Mechanical Engineering and Naval Architecture, University of Split, Split, Croatia*
- ³⁴ *Faculty of Nuclear Sciences and Physical Engineering, Czech Technical University in Prague, Prague, Czech Republic*
- ³⁵ *Faculty of Physics, Sofia University, Sofia, Bulgaria*
- ³⁶ *Faculty of Science, P.J. Šafárik University, Košice, Slovak Republic*
- ³⁷ *Faculty of Technology, Environmental and Social Sciences, Bergen, Norway*
- ³⁸ *Frankfurt Institute for Advanced Studies, Johann Wolfgang Goethe-Universität Frankfurt, Frankfurt, Germany*
- ³⁹ *Fudan University, Shanghai, China*
- ⁴⁰ *Gangneung-Wonju National University, Gangneung, Republic of Korea*
- ⁴¹ *Gauhati University, Department of Physics, Guwahati, India*
- ⁴² *Helmholtz-Institut für Strahlen- und Kernphysik, Rheinische Friedrich-Wilhelms-Universität Bonn, Bonn, Germany*
- ⁴³ *Helsinki Institute of Physics (HIP), Helsinki, Finland*
- ⁴⁴ *High Energy Physics Group, Universidad Autónoma de Puebla, Puebla, Mexico*
- ⁴⁵ *Horia Hulubei National Institute of Physics and Nuclear Engineering, Bucharest, Romania*
- ⁴⁶ *HUN-REN Wigner Research Centre for Physics, Budapest, Hungary*
- ⁴⁷ *Indian Institute of Technology Bombay (IIT), Mumbai, India*
- ⁴⁸ *Indian Institute of Technology Indore, Indore, India*
- ⁴⁹ *INFN, Laboratori Nazionali di Frascati, Frascati, Italy*
- ⁵⁰ *INFN, Sezione di Bari, Bari, Italy*
- ⁵¹ *INFN, Sezione di Bologna, Bologna, Italy*
- ⁵² *INFN, Sezione di Cagliari, Cagliari, Italy*
- ⁵³ *INFN, Sezione di Catania, Catania, Italy*
- ⁵⁴ *INFN, Sezione di Padova, Padova, Italy*
- ⁵⁵ *INFN, Sezione di Pavia, Pavia, Italy*
- ⁵⁶ *INFN, Sezione di Torino, Turin, Italy*
- ⁵⁷ *INFN, Sezione di Trieste, Trieste, Italy*
- ⁵⁸ *Inha University, Incheon, Republic of Korea*
- ⁵⁹ *Institute for Gravitational and Subatomic Physics (GRASP), Utrecht University/Nikhef, Utrecht, Netherlands*
- ⁶⁰ *Institute of Experimental Physics, Slovak Academy of Sciences, Košice, Slovak Republic*
- ⁶¹ *Institute of Physics, Homi Bhabha National Institute, Bhubaneswar, India*
- ⁶² *Institute of Physics of the Czech Academy of Sciences, Prague, Czech Republic*
- ⁶³ *Institute of Space Science (ISS), Bucharest, Romania*
- ⁶⁴ *Institut für Kernphysik, Johann Wolfgang Goethe-Universität Frankfurt, Frankfurt, Germany*
- ⁶⁵ *Instituto de Ciencias Nucleares, Universidad Nacional Autónoma de México, Mexico City, Mexico*

- ⁶⁶ *Instituto de Física, Universidade Federal do Rio Grande do Sul (UFRGS), Porto Alegre, Brazil*
- ⁶⁷ *Instituto de Física, Universidad Nacional Autónoma de México, Mexico City, Mexico*
- ⁶⁸ *iThemba LABS, National Research Foundation, Somerset West, South Africa*
- ⁶⁹ *Jeonbuk National University, Jeonju, Republic of Korea*
- ⁷⁰ *Johann-Wolfgang-Goethe Universität Frankfurt Institut für Informatik, Fachbereich Informatik und Mathematik, Frankfurt, Germany*
- ⁷¹ *Korea Institute of Science and Technology Information, Daejeon, Republic of Korea*
- ⁷² *KTO Karatay University, Konya, Turkey*
- ⁷³ *Laboratoire de Physique Subatomique et de Cosmologie, Université Grenoble-Alpes, CNRS-IN2P3, Grenoble, France*
- ⁷⁴ *Lawrence Berkeley National Laboratory, Berkeley, California, U.S.A.*
- ⁷⁵ *Lund University Department of Physics, Division of Particle Physics, Lund, Sweden*
- ⁷⁶ *Marietta Blau Institute, Vienna, Austria*
- ⁷⁷ *Nagasaki Institute of Applied Science, Nagasaki, Japan*
- ⁷⁸ *Nara Women's University (NWU), Nara, Japan*
- ⁷⁹ *National and Kapodistrian University of Athens, School of Science, Department of Physics, Athens, Greece*
- ⁸⁰ *National Centre for Nuclear Research, Warsaw, Poland*
- ⁸¹ *National Institute of Science Education and Research, Homi Bhabha National Institute, Jatni, India*
- ⁸² *National Nuclear Research Center, Baku, Azerbaijan*
- ⁸³ *National Research and Innovation Agency - BRIN, Jakarta, Indonesia*
- ⁸⁴ *Niels Bohr Institute, University of Copenhagen, Copenhagen, Denmark*
- ⁸⁵ *Nikhef, National institute for subatomic physics, Amsterdam, Netherlands*
- ⁸⁶ *Nuclear Physics Group, STFC Daresbury Laboratory, Daresbury, U.K.*
- ⁸⁷ *Nuclear Physics Institute of the Czech Academy of Sciences, Husinec-Řež, Czech Republic*
- ⁸⁸ *Oak Ridge National Laboratory, Oak Ridge, Tennessee, U.S.A.*
- ⁸⁹ *Ohio State University, Columbus, Ohio, U.S.A.*
- ⁹⁰ *Physics department, Faculty of science, University of Zagreb, Zagreb, Croatia*
- ⁹¹ *Physics Department, Panjab University, Chandigarh, India*
- ⁹² *Physics Department, University of Jammu, Jammu, India*
- ⁹³ *Physics Program and International Institute for Sustainability with Knotted Chiral Meta Matter (WPI-SKCM²), Hiroshima University, Hiroshima, Japan*
- ⁹⁴ *Physikalisches Institut, Eberhard-Karls-Universität Tübingen, Tübingen, Germany*
- ⁹⁵ *Physikalisches Institut, Ruprecht-Karls-Universität Heidelberg, Heidelberg, Germany*
- ⁹⁶ *Physik Department, Technische Universität München, Munich, Germany*
- ⁹⁷ *Politecnico di Bari, Bari, Italy*
- ⁹⁸ *Research Division and ExtreMe Matter Institute EMMI, GSI Helmholtzzentrum für Schwerionenforschung GmbH, Darmstadt, Germany*
- ⁹⁹ *Saga University, Saga, Japan*
- ¹⁰⁰ *Saha Institute of Nuclear Physics, Homi Bhabha National Institute, Kolkata, India*
- ¹⁰¹ *School of Physics and Astronomy, University of Birmingham, Birmingham, U.K.*
- ¹⁰² *Sección Física, Departamento de Ciencias, Pontificia Universidad Católica del Perú, Lima, Peru*
- ¹⁰³ *SUBATECH, IMT Atlantique, Nantes Université, CNRS-IN2P3, Nantes, France*
- ¹⁰⁴ *Sungkyunkwan University, Suwon City, Republic of Korea*
- ¹⁰⁵ *Suranaree University of Technology, Nakhon Ratchasima, Thailand*
- ¹⁰⁶ *Technical University of Košice, Košice, Slovak Republic*
- ¹⁰⁷ *The Henryk Niewodniczanski Institute of Nuclear Physics, Polish Academy of Sciences, Cracow, Poland*
- ¹⁰⁸ *The University of Texas at Austin, Austin, Texas, U.S.A.*
- ¹⁰⁹ *Universidad Autónoma de Sinaloa, Culiacán, Mexico*
- ¹¹⁰ *Universidade de São Paulo (USP), São Paulo, Brazil*
- ¹¹¹ *Universidade Estadual de Campinas (UNICAMP), Campinas, Brazil*
- ¹¹² *Universidade Federal do ABC, Santo Andre, Brazil*
- ¹¹³ *Universitatea Nationala de Stiinta si Tehnologie Politehnica Bucuresti, Bucharest, Romania*
- ¹¹⁴ *University of Cape Town, Cape Town, South Africa*

- ¹¹⁵ *University of Derby, Derby, U.K.*
- ¹¹⁶ *University of Houston, Houston, Texas, U.S.A.*
- ¹¹⁷ *University of Jyväskylä, Jyväskylä, Finland*
- ¹¹⁸ *University of Kansas, Lawrence, Kansas, U.S.A.*
- ¹¹⁹ *University of Liverpool, Liverpool, U.K.*
- ¹²⁰ *University of Science and Technology of China, Hefei, China*
- ¹²¹ *University of South-Eastern Norway, Kongsberg, Norway*
- ¹²² *University of Tennessee, Knoxville, Tennessee, U.S.A.*
- ¹²³ *University of the Witwatersrand, Johannesburg, South Africa*
- ¹²⁴ *University of Tokyo, Tokyo, Japan*
- ¹²⁵ *University of Tsukuba, Tsukuba, Japan*
- ¹²⁶ *Universität Münster, Institut für Kernphysik, Münster, Germany*
- ¹²⁷ *Université Clermont Auvergne, CNRS/IN2P3, LPC, Clermont-Ferrand, France*
- ¹²⁸ *Université de Lyon, CNRS/IN2P3, Institut de Physique des 2 Infinis de Lyon, Lyon, France*
- ¹²⁹ *Université de Strasbourg, CNRS, IPHC UMR 7178, F-67000 Strasbourg, France, Strasbourg, France*
- ¹³⁰ *Université Paris-Saclay, Centre d'Etudes de Saclay (CEA), IRFU, Département de Physique Nucléaire (DPhN), Saclay, France*
- ¹³¹ *Université Paris-Saclay, CNRS/IN2P3, IJCLab, Orsay, France*
- ¹³² *Università degli Studi di Foggia, Foggia, Italy*
- ¹³³ *Università del Piemonte Orientale, Vercelli, Italy*
- ¹³⁴ *Università di Brescia, Brescia, Italy*
- ¹³⁵ *Variable Energy Cyclotron Centre, Homi Bhabha National Institute, Kolkata, India*
- ¹³⁶ *Warsaw University of Technology, Warsaw, Poland*
- ¹³⁷ *Wayne State University, Detroit, Michigan, U.S.A.*
- ¹³⁸ *Yale University, New Haven, Connecticut, U.S.A.*
- ¹³⁹ *Yonsei University, Seoul, Republic of Korea*
- ¹⁴⁰ *Affiliated with an institute formerly covered by a cooperation agreement with CERN*
- ¹⁴¹ *Affiliated with an international laboratory covered by a cooperation agreement with CERN.*
- ^a *Also at Max-Planck-Institut für Physik, Munich, Germany*
- ^b *Also at Czech Technical University in Prague (CZ)*
- ^c *Also at Italian National Agency for New Technologies, Energy and Sustainable Economic Development (ENEA), Bologna, Italy*
- ^d *Also at Dipartimento DET del Politecnico di Torino, Turin, Italy*
- ^e *Also at Department of Applied Physics, Aligarh Muslim University, Aligarh, India*
- ^f *Also at Institute of Theoretical Physics, University of Wrocław, Poland*
- ^g *Also at Facultad de Ciencias, Universidad Nacional Autónoma de México, Mexico City, Mexico*
- [†] *Deceased*